Journal of Asian Earth Sciences 188 (2020) 104097

Contents lists available at ScienceDirect

Journal of Asian Earth Sciences

journal homepage: www.elsevier.com/locate/jseaes

Full length article

Possible Lithosphere-Atmosphere-Ionosphere Coupling effects prior to the 2018 Mw = 7.5 Indonesia earthquake from seismic, atmospheric and ionospheric data

Dedalo Marchetti[a,b], Angelo De Santis[b,*], Xuhui Shen[c], Saioa A. Campuzano[b], Loredana Perrone[b], Alessandro Piscini[b], Rita Di Giovambattista[b], Shuanggen Jin[a], Alessandro Ippolito[b,d], Gianfranco Cianchini[b], Claudio Cesaroni[b], Dario Sabbagh[b], Luca Spogli[b,e], Zeren Zhima[c], Jianping Huang[c]

[a] School of Remote Sensing and Geomatics Engineering, Nanjing University of Information Science and Technology, Nanjing 210044, China
[b] INGV – Istituto Nazionale di Geofisica e Vulcanologia (National Institute of Geophysics and Volcanology), Rome, Italy
[c] Institute of Crustal Dynamics, China Earthquake Administration, Beijing, China
[d] ASI, Italian Space Agency, Rome, Italy
[e] SpacEarth Technology, Rome, Italy

ARTICLE INFO

Keywords:
Seismic precursors
LAIC
Ionospheric electron density
Geomagnetic field
Swarm satellites
CSES mission

ABSTRACT

In this study, we analyse Lithosphere Atmosphere Ionosphere Coupling (LAIC) effects to identify some phenomena that could, possibly, be linked to the preparation phase of the $M_W = 7.5$ earthquake occurred in Indonesia on September 28th, 2018, by investigating the eight months preceding the seismic event.

First, we find a seismic acceleration that started two months before the mainshock. Then, studying some physical properties of the atmosphere (skin temperature, total column water vapor and aerosol optical thickness), we find two increases of atmospheric anomalies about 6 and 3.7 months before the mainshock, and the latter one is very promising as a candidate for seismic-related phenomena. Furthermore, we investigate ionospheric disturbances, by analysing the Swarm and, for the first time, China Seismo-Electromagnetic Satellite (CSES), magnetic and electron density data during quiet geomagnetic time. From different techniques, we find interesting anomalies concentrated around 2.7 months before the mainshock.

On August 19th, 2018, Swarm and CSES showed an enhancement of the electron density during night time. We critically discuss the possibility that such phenomenon can be a possible pre-seismic-induced ionospheric effect.

Finally, we performed a cumulative analysis using all detected anomalies, as a test case for a possible chain of physical phenomena that could happen before the earthquake occurrence. With this study, we support the usefulness to collect and store large Earth ground and satellite observational dataset that in the future could be useful to monitor in real time the seismic zones to anticipate earthquakes, although nowadays, there is no evidence about useful prediction capabilities.

1. Introduction

On September 28th, 2018 at 10:02:45 UTC a 7.5 moment magnitude (Mw) earthquake occurred in Indonesia (0.256°S 119.845°E) with a hypocentre at 20 km of depth. In the earthquake region, the tectonic movements are complex and involve both convergence of big plates (e.g. Australia, Sunda, Pacific, and Philippine Sea plates) and smaller movements of microplates (Zhang et al., 2017). Fig. 1 shows the geographical position where the event occurred (a), the other earthquakes happened in previous five years with some geographical and tectonic settings (b) and a graph of the cumulative number of earthquakes (c). The earthquake epicenter is between the Molucca Sea microplate and Sunda tectonic plate. The Molucca sea plate, among the particular features, is between two subduction zones. Focal mechanism indicates strike-slip faulting within the interior of the Molucca Sea microplate, part of the broader Sunda tectonic plate. Ground shaking of

* Corresponding author.
E-mail address: angelo.desantis@ingv.it (A. De Santis).

https://doi.org/10.1016/j.jseaes.2019.104097
Received 28 June 2019; Received in revised form 16 October 2019; Accepted 18 October 2019
Available online 26 October 2019
1367-9120/

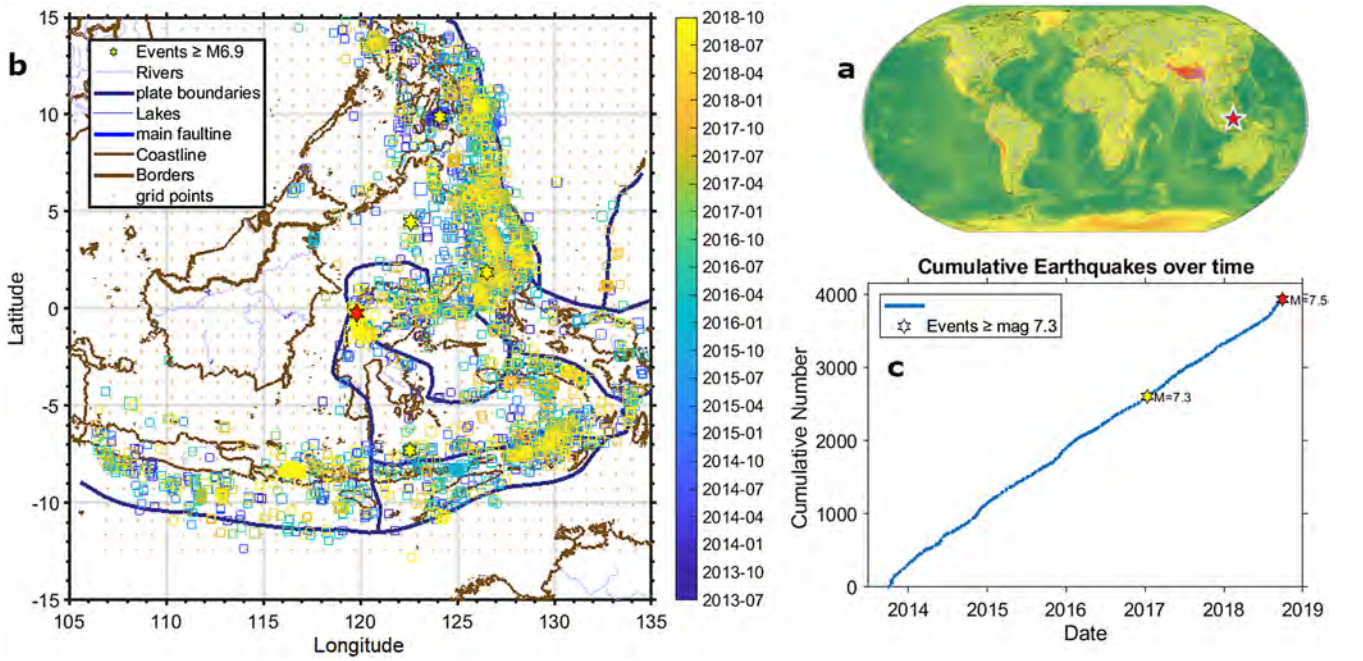

Fig. 1. Seismic context for the Mw = 7.5 Palu (Indonesia) earthquake. (a) Localization of the earthquake epicenter in the World map. (b) Map of the earthquakes occurred from September 28th, 2013 to September 28th, 2018 with magnitude equal to or greater than 4.5 from USGS catalog (USGS, 2018). The colour is related to the origin time. The map shows the main plate boundaries and some geographical elements. (c) Graph of the cumulative number of earthquakes in function of the time. Stars represent the two M7.3 + earthquakes. The Mw = 7.5 Palu (Indonesia) September 28th, 2018 earthquake is represented in all panels a, b and c by a red star. (For interpretation of the references to colour in this figure legend, the reader is referred to the web version of this article.)

the earthquake produced extensive damage to about 680,000 houses and unfortunately at least 2103 victims and 4612 injured people (USGS, 2018).

Despite today there is no clearly established evidence for earthquake precursor phenomena, in the last decade many studies have been conducted to search for possible physical and chemical alterations which could be related with the earthquake occurrence (see e.g. Cicerone et al., 2009; De Santis et al., 2015a). In many occasions, unexpected changes in some geophysical quantities have been found, but they could not be linked with certainty to a given earthquake.

Many works suggest possible pre-earthquake anomalies for the observables that we investigate in this paper (i.e. the seismicity rate, atmospheric perturbations and ionospheric electron density and magnetic field alterations). A seismic study of the Mw = 6.2 destructive Italian earthquake of L'Aquila April, 6th, 2009 was reported by De Santis et al. (2015b). Atmospheric alterations, for example of surface temperature, were reported by Aliano et al. (2008) and Tramutoli (2015) in two statistical studies of different earthquakes, while aerosol anomalies prior to Mw = 7.8 Wenchuan and Mw = 6.6 Lushan earthquakes were detected by Liu et al. (2019). Ionospheric electron density enhancement before large earthquakes was reported from ground measurements by GNSS stations (e.g. Heki, 2011; Kamogawa and Kakinami, 2013), and from DEMETER satellite (Nêmec et al., 2008; Akhoondzadeh et al. 2010a and 2010b; He et al., 2011; Piša et al., 2013; Li and Parrot, 2013; Parrot, 2013; Parrot and Li 2015; Yan et al., 2017). Electromagnetic emissions were also reported for some significant earthquakes in the world from ground geomagnetic observatories (e.g. Fraser-Smith et al., 1990; Molchanov et al., 1992; Donner et al., 2015).

The most recent studies in this field pointed to the importance of collecting and coherently analysing as many data from different sources as possible and investigated many parts of the Earth system, i.e. a geosystemic study, as described by De Santis et al. (2015a, 2019).

More analyses applied to different case studies were successfully conducted using Swarm satellite magnetic data, by finding a possible relation between the ionospheric magnetic anomalies and earthquake occurrence. The case studies investigated following this approach were the Nepal Mw = 7.8 2015 (De Santis et al., 2017), Ecuador Mw = 7.8 2016 (Akhoondzadeh et al., 2018), and Mexico Mw = 8.2 2017 (Marchetti and Akhoondzadeh, 2018) earthquakes, as well as Central Italy seismic sequence 2016–2017 (Marchetti et al., 2019a). Perturbations in the atmosphere (i.e. skin temperature, total column water vapor and total column ozone) before the main events of the last 22 years in Central Italy were also observed, as, in particular, prior to the start of the 2016–2017 Central Italy seismic sequence (Piscini et al., 2017). An associated 22-year statistics was also performed, establishing the robustness of the analysed atmospheric parameters as earthquake precursors, at least for the region of study.

In this paper, we investigate the preparatory phase of the Mw = 7.5 Indonesia September 28th, 2018 earthquake searching for Lithosphere Atmosphere Ionosphere Coupling (LAIC) effects as described by different models (e.g. Freund et al., 2011, Kuo et al., 2014, Pulinets and Ouzounov, 2011). Section 2 presents the analysed dataset; in particular, the China Seismo Electromagnetic Satellite (CSES; Shen et al., 2018) is described in detail as it is the first time that we investigate the data of this new satellite. Section 3 presents the data analysis methods and the results proceeding in the "natural order" from the bottom to the top: lithosphere in 3.1, atmosphere in 3.2 and finally ionosphere in 3.3. Section 4 provides a common view of the analysis along with a discussion and Section 5 reports some conclusions.

2. Dataset

2.1. Seismic data

The seismic data are extracted from the USGS earthquake catalogue (USGS, 2018). The USGS catalogue has a worldwide coverage collecting and analysing data from a worldwide network of seismometers. We extract the earthquake data from five years before the Mw7.5 Indonesia 2018 earthquake. The earthquake database is composed of date, time, location (geographic coordinates, depth) and magnitude, at least 4.5 around the region of interest, to be sufficiently above the magnitude of completeness M_C (Kagan and Yan, 2003).

2.2. CSES satellite data

CSES (China Seismo Electromagnetic Satellite) mission is a China satellite constellation devoted to the research of possible earthquake-related electromagnetic phenomena. On February, 2nd 2018 the first satellite, CSES ZhangHeng-01 was successfully launched and it is still in orbit (Shen et al., 2018). CSES-01 hosts nine scientific payloads, among them fluxgate magnetometers, absolute scalar magnetometer, Langmuir probes, and two particle detectors. One of them, the HEPD, is provided by INFN (Italian National Institute of Nuclear Physics; Alfonsi et al., 2017) with support of the Italian Space Agency (ASI). The CSES-01 satellite is placed at an altitude of about 505 km in a quasi-polar Sun-synchronous orbit. The satellite passes at about 2 AM and 2 PM of local time in its ascending and descending orbits, respectively. Its revisited time is about 5 days.

In this paper, we analyse the electron density measured by Langmuir Probes (LAP) and vector magnetic field measured by High Precision Magnetometer (HPM), both on-board CSES satellite. Data are available to us only for the months April, August and September 2018. Although the period is limited, we think they are sufficient for the present study. Before proceeding to search for electromagnetic signals potentially related to the seismic activity, we performed a series of checks on the data.

In-situ measurements of plasma parameters at the satellite altitude are performed mainly by Langmuir Probes and Plasma Analyzer Package (Yan et al., 2018). Electron density estimated by CSES Langmuir probe is provided in the LAP Level 02 product with a time resolution of 3 s. Each file contains one semi-orbit (ascending or descending) of the satellite. The files are provided in the HDF Version 5 data format. Unfortunately, not all files contain the same information fields. In particular, some of them do not include the Flag field, which provides information about the quality of the data. In each file, the first two columns contain the electron density (Ne), in number of electrons per cubic meter, and electron temperature (Te), in Kelvin, the other columns contain flag (if present), geographical and geomagnetic coordinates, and Universal Time Clock (UTC) of data acquisition.

Therefore, we developed a suitable software that converts the data format to one standard and checks for possible issues inside the original Level 02 data.

The Ne and Te samples with unphysical values are not considered in this work. We adopted a conservative strategy and decided to exclude the whole track that contained one or more negative samples of Ne, as we do not know if the problem is confined to the single sample or extended to the whole satellite track.

We also analysed the available data from High Precision magnetometer (HPM) instrument (Cheng et al., 2018). CSES satellite is equipped by two fluxgate magnetometers placed at the final part of a specific boom. One boom is perpendicular with respect to the other one. The orientation of the spacecraft is determined by the star-camera system placed on the body of the satellite; unfortunately, there is no instrument to know eventual differences in positions of the magnetometers with respect to the spacecraft platform, due, for example, to vibrations, deformations of structure and so on. Despite this, we do not expect troubles for this study due to the little uncertainty in the absolute orientation of the magnetic vector instruments. For possible seismic precursors from electromagnetic satellite, the East (Y) component of the magnetic field seems more promising (Pinheiro et al., 2011, De Santis et al., 2017, Marchetti et al., 2019a).

2.3. Swarm satellite data

The European Space Agency (ESA) Swarm satellite mission has been successfully orbiting since November 2013. The main goal of the mission, composed of three identical satellites, is to monitor the geomagnetic field and its variations (e.g. Friis-Christensen et al., 2006). Each satellite is equipped with scalar and vector magnetometers. In addition, there is aboard some complementary instrumentation such as Langmuir Probe, Thermal Ion Imager, accelerometers, laser retroreflectors and so on, to monitor the ionospheric plasma density, temperature, composition, gravitational field anomalies and to precisely determine the position of the satellites, respectively. The three twin satellites are called Alpha, Bravo, and Charlie. The orbital configuration is selected to achieve different goals of the Swarm mission: Alpha and Charlie satellites fly close each other at a separation of about 150 km at an altitude of about 445 km (at September 2018) and Bravo satellite is on a higher orbit of about 510 km (at September 2018).

Recently, ESA joined in the constellation a fourth satellite, the Canadian satellite CASSIOPE, already flying from September 2013, with the scientific payload e-POP composed by fluxgate magnetometers and other instruments.

Swarm data are provided by ESA with 3–4 days of delay from acquisition time. In this paper, we investigate the magnetic field data provided by the magnetic low resolution (1 Hz) Level-1b product version 505, called MAGx_LR, and the plasma data from EFIx_LP Level-1b product version 403, that provides Ne, Te and spacecraft potential with a sample rate of 2 Hz.

2.4. Climatological data

To investigate possible alterations in the atmosphere preceding the earthquake, we use some climatological data from ERA-Interim and IFS/Analysis provided by the European Center for Medium-Range Weather Forecast (ECMWF) and from MERRA-2 (Modern-Era Retrospective analysis for Research and Applications, Version 2) dataset provided by NASA (Dee et al., 2011; Gelaro et al., 2017). ERA-Interim and MERRA-2 are two climatological models based on real observations from ground, airplanes, balloons and satellites. Each model applies the same own strategy along a large time scale guarantying as much as possible the homogeneity of the data also where the acquisition instruments are different in quality and number. Therefore, despite the datasets are based on real data points, the provided climatological and meteorological quantities are estimated on a fixed spatial grid with at specific time resolution.

In analogy to the availability of new satellite mission CSES, we extract the climatological data from February, 2nd 2018 (the day of the launch of CSES) to September, 28th 2018 (the earthquake day). In particular, we investigate skin temperature (skt) and total column water vapor (tcwv) from ECMWF and Aerosol Optical Thickness (AOT) from MERRA-2. To estimate the historical means of the selected parameters, we extract all the available data of each dataset: from 1979 (for ERA-Interim) and from 1980 (for MERRA-2) until 2017 for the same months/days. The data are extracted in a squared region surrounding the earthquake with a size defined by the Dobrovolsky's radius (Dobrovolsky et al., 1979) and equal in kilometres to $10^{0.43M}$, with M the magnitude of the earthquake. In this case, the squared region has a side of about 1680 km.

3. Data analysis and results

Here, we will discuss the methods for data processing as applied to the described datasets in the Section 2. This section applies different approaches to different dataset types: 3.1 is dedicated to seismological data analysis, searching for a possible seismic acceleration; in section 3.2 we investigate the atmospheric physical characteristics to detect possible pre-earthquake anomalies; CSES Ne and magnetic data investigation for possible enhancement of ionospheric electron density and possible disturbances above the earthquake region is provided in Sections 3.3–3.5; Section 3.6 presents a combined analysis of electron density measurements acquired by Swarm constellation with CSES satellite for deep investigation of the features of an ionospheric anomaly reported in the investigated period; finally Section 3.7 presents the Swarm magnetic field investigation in the area during the 8 months

Table 1
List of the earthquakes with magnitude M ≥ 5.5 happened in chronological order inside Dobrovolsky's area of Mw7.5 September 28th, 2018 Indonesia earthquake from February 2nd, 2018 to September 28th, 2018.

Year	Month	Day	UT Hour	minute	Latitude	Longitude	Depth	Magnitude
2018	2	2	0	20	−0.247	125.182	38	5.5
2018	2	26	13	34	−2.777	126.686	9	6.1
2018	3	8	3	51	−3.343	130.934	10	5.6
2018	4	5	3	53	6.832	126.778	34	6
2018	4	15	19	30	1.408	126.876	34	6
2018	4	17	2	52	−3.522	131.303	10	5.5
2018	5	10	11	56	10.172	125.637	29	5.7
2018	6	2	16	28	4.587	126.657	23	5.7
2018	7	28	22	47	−8.239	116.508	14	6.4
2018	8	5	11	46	−8.258	116.438	34	6.9
2018	8	5	12	49	−8.358	116.14	31	5.5
2018	8	9	5	25	−8.306	116.23	15	5.9
2018	8	19	4	10	−8.337	116.599	16	6.3
2018	8	19	14	56	−8.319	116.627	21	6.9
2018	8	19	15	4	−8.284	116.594	10	5.6
2018	8	19	15	16	−8.351	116.557	10	5.8
2018	8	19	15	28	−8.391	116.557	10	5.5
2018	8	25	18	33	−8.422	116.926	12	5.5
2018	8	28	7	8	−10.773	124.187	14	6.2
2018	8	28	7	13	−10.631	124.136	8	5.7
2018	9	8	7	16	7.238	126.478	10	6.2
2018	9	28	6	59	−0.399	119.77	5	6.1
2018	9	28	10	2	−0.256	119.845	20	7.5
2018	9	28	10	14	−0.018	119.755	10	5.8
2018	9	28	10	16	−0.875	120.034	10	5.7
2018	9	28	10	25	−1.047	119.935	10	5.8
2018	9	28	10	50	−0.781	119.915	10	5.6
2018	9	28	11	6	−1.503	120.058	10	5.6
2018	9	28	13	35	0.058	119.682	10	5.7

before the occurrence of the earthquake.

3.1. Seismological investigation

From a tectonic point of view, the location of the Mw7.5 September 28th, 2018 Indonesia earthquake is one of the most complexes of the world, as the region is a complex convergence place of many different plates (e.g. Australia, Sunda, Pacific, and Philippine Sea Plates). Therefore, seismological studies must be performed with a careful analysis and control of influence of each tectonic process.

Fig. 1b shows the geographical map distribution of the earthquakes occurred from September 28th, 2013 to September 28th, 2018 extracted from USGS catalog (USGS, 2018) with magnitude equal to or greater than 4.5. Fig. 1c shows the cumulative number of the earthquakes. This curve does not present any peculiar aspect due to the wide region under investigation, in which the seismic rate of M4.5+ earthquakes is almost constant. For providing an idea of the intense seismicity, Table 1 reports the list of the earthquakes with magnitude equal to or greater than 5.5 (considering 4.5 would have provided a too long list) happened inside Dobrovolsky's area of the Mw7.5 September 28th, 2018 earthquake from February, 2nd 2018 (the launch of CSES satellite) to the day of the mainshock.

The first processing of the data is to select the shallow earthquakes defined by a maximum hypocentral depth of 50 km. This selection is based on two main reasons: the first is that the Mw7.5 event is shallow, being its depth of (20.0 ± 1.8) km (USGS, 2018); the second is related to the fact that deeper earthquakes are less reliable to produce some LAIC effects (e.g. Molchanov and Hayakawa, 2008). For a reliable seismic analysis it is fundamental to perform some check on the earthquake catalogue. The most important is the estimation of the magnitude of completeness, i.e. that all seismic events with that magnitude and larger in the area and time under analysis are detected by the used seismic network. A test of the Magnitude of Completeness by means of ZMAP (Wiemer, 2001) confirms that the catalog is complete at least from the magnitude 4.5 for the shallow earthquakes occurred in this region and time.

For each selected seismic event we computed the released energy in Joule (e.g. Kanamori and Anderson, 1975; Han et al., 2014)

$$E_i(J) = 10^{(1.5M_i+4.8)} \quad (1)$$

where M_i is the magnitude of the "i-th" earthquake. The search for a possible seismic acceleration is performed by means of the Accelerating Moment Release (AMR) technique as described by Mignan et al. (2007), in particular by calculating the cumulative Benioff strain S:

$$S = \sum_i \sqrt{E_i} \quad (2)$$

Fig. 2 shows the quantity S for earthquakes inside the Dobrovolsky's radius at a maximum depth of 50 km starting from January, 1st, 2018 until the September 28th, 2018, i.e. the day of the Mw7.5 earthquake. The Mw7.5 mainshock and subsequent aftershocks were excluded from this analysis, to test if the seismicity that preceded the mainshock could predict, in such way, its occurrence.

The cumulative Benioff strain (Fig. 2a) showed a quasi-linear trend until July 28th, 2018. On this day, an M6.4 earthquake occurred at 8.239° S and 116.508° E, 14 km depth (Table 1). After this event, the slope of the curve increased by depicting a seismic activation of the region under investigation. To verify this feature, we subtract the linear trend calculated from January 1st, 2018 to July 27th, 2018 obtaining the residuals presented in Fig. 2b. We can see that in these first seven months there are up and down trends that probably correspond to some periods of more released seismic energy followed by others of seismic relaxation. From July 28th, 2018 until the end, the residuals are only increased, and, in about a week, the residuals overpass three standard deviations, i.e. the upper red band on the graph (that is estimated as the sum of squares of the residuals after removing the linear fit). After July 28th, 2018, the residual strain did not ever come back inside this 3-sigma threshold, so from this point we can affirm that the system passes from a linear phase to a complex-chaotic phase, i.e. a seismic activation of the region started exactly 2 months before the mainshock.

Furthermore, the very last part of the cumulative released strain

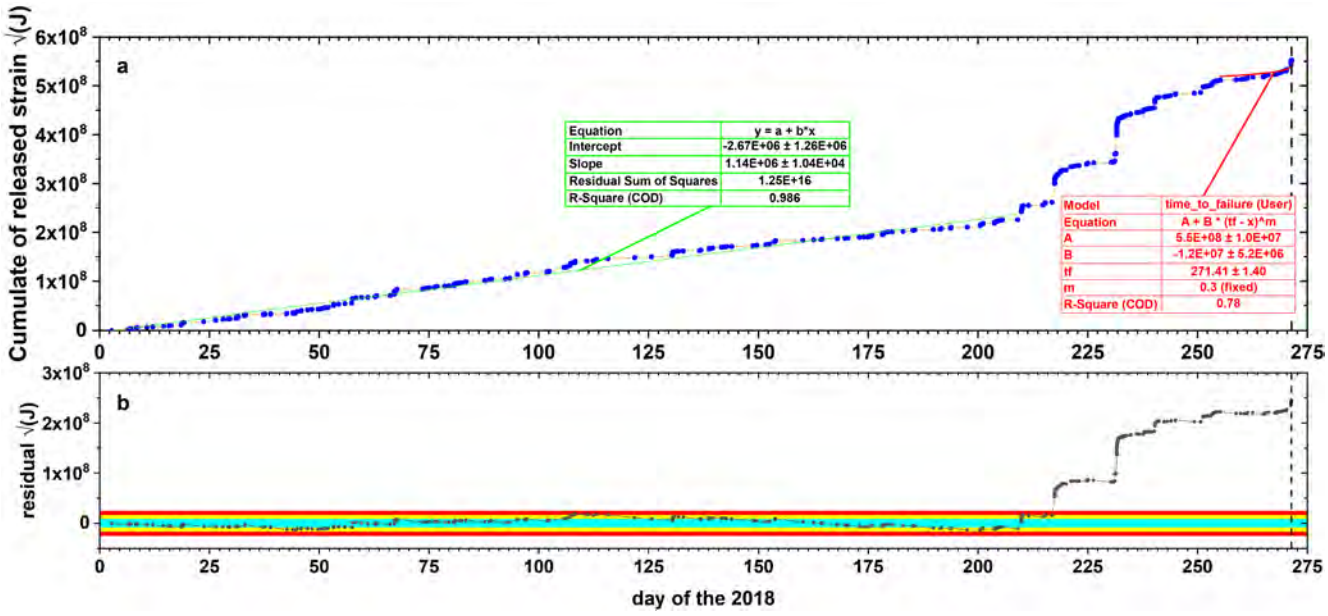

Fig. 2. (a) Cumulative released strain for shallow (depth ≤ 50 km) earthquakes from January 1st, 2018 until the Mw7.5 September 28th, 2018 earthquake (excluded from this calculus and graph). (b) AMR analysis: residual of the cumulate minus the linear fit (green line in upside graph). Thresholds as 1.0, 2.0 and 3.0 standard deviations are plotted as cyan, yellow and red horizontal bands, respectively. (For interpretation of the references to colour in this figure legend, the reader is referred to the web version of this article.)

presents a remarkable acceleration, started some days before the mainshock. We superpose a non-linear power law fit made by a typical Accelerated Moment Release (De Santis et al., 2015b, Eq. (3)), fixing the exponent to 0.3 on the last 16 days of the trend. The fit confirms the final acceleration with a time of failure on the same day of the earthquake (September, 28th 2018) just six minutes before the mainshock (9:56:06). We underline that the mainshock was not used to make this fit. The result is promising for a future real-time monitor platform taking into account also the possible improvement of the AMR technique (see for instance De Santis et al., 2015b). Nevertheless, it is worth recalling that it is well known that some devastating earthquakes could not be preceded by foreshocks or seismic acceleration (e.g. Italian Amatrice M6.0 earthquake of 2016; Marchetti et al., 2019b).

3.2. Climatological analysis

The meteorological/climatological selected parameters (skt, tcwv and AOT) are extracted for the analysed period, i.e. from February 2nd to September 28th for each year from 1979 (or 1980 for AOT) to 2018, from ECMWF and MERRA-2 datasets (see Section 2 for more details about the data). The data are extracted in a square centred on the earthquake epicenter with a side of 3°. This size is selected as a compromise between the size of the impending fault and the Dobrovolsky's area, being the former too small and the latter too vast to search for possible chemical and heating emissions from the ground (e.g. Tramutoli, 2015 reports thermal anomaly along the fault but also at several hundred km of distance from the epicentre). Each day is separately analysed from 1979 (or 1980 for AOT) to 2017, estimating the mean value and its standard deviation for the investigated parameter, i.e. in the whole time period but excluding the year of earthquake (2018 in this case). The skt and tcwv are considered only on land by a filter with a land-sea mask extracted from the same ECMWF archive, as, in particular for skt, the sea is not sensible to small local heating due to his great heat capacity. The small size of the islands in this region compared with the resolution of the ECMWF dataset (0.5°) forced us to include a small portion of the sea and to exclude some small islands.

The time series of the mean values in the analysed period forms the historical time series. For skt and tcwv, any long trend variations (as a possible "global warming") is removed by the CAPRI algorithm as described by Piscini et al. (2017, 2019). Then, the values of the year of the earthquake (2018) are superposed to the historical time series, by checking if there are some days that exceed the upper bound produced by two standard deviations from the mean values and we tag these days as "anomalous".

Fig. 3 shows the climatological analysis for the Mw7.5 September 28th, 2018 Indonesia earthquake. A dashed red line represents the parameter values in the earthquake year, the historical time series and its 1.0, 1.5 and 2.0 standard deviations are represented by a blue line, cyan, green and yellow bands, respectively. We underline by red circles the values that exceed two standard deviations, i.e. the anomalous days.

We detect some anomalous days in skin temperature, atmospheric water vapor and aerosol. The skin temperature presents two anomalous days on June 9th and on July 28th, 2018. We note that the latter coincides with the seismological activation, so we could infer that the geosystemic system acts as a whole interconnected system where subsystems are connected, that is very promising for the multi-approach and multi-parametric study analysis. Total column water vapor presents only one anomaly on May 29th, 2018. The aerosol analysis detects several anomalous days with some that persist for two or more days: February 5th, April 1st – 2nd – 3rd, 8th, and 30th, June 5th – 6th, 8th, 11th, and August 2nd. In the supplementary material, we provide an animation that shows the locations of anomalous pixels inside the Dobrovolsky's area and the amount of overpassing the thresholds starting from three months before the earthquake until the event. We notice that the August 2nd, 2018 anomaly is the closest to the future earthquake epicentre.

3.3. CSES electron density characterization and research for positive anomalies

The objective of this analysis is to search for a possible increase of the electron density and deviations from the expected day-to-day variability of the Equatorial Ionospheric Anomaly (EIA). EIA is a typical daytime feature of the low-latitude ionosphere, appearing as two peaks of Ne at about ± 15/20 geomagnetic latitude degrees (e.g. Hanson and Moffet, 1966; MacDouglas, 1969; Walker et al., 1994), that are known

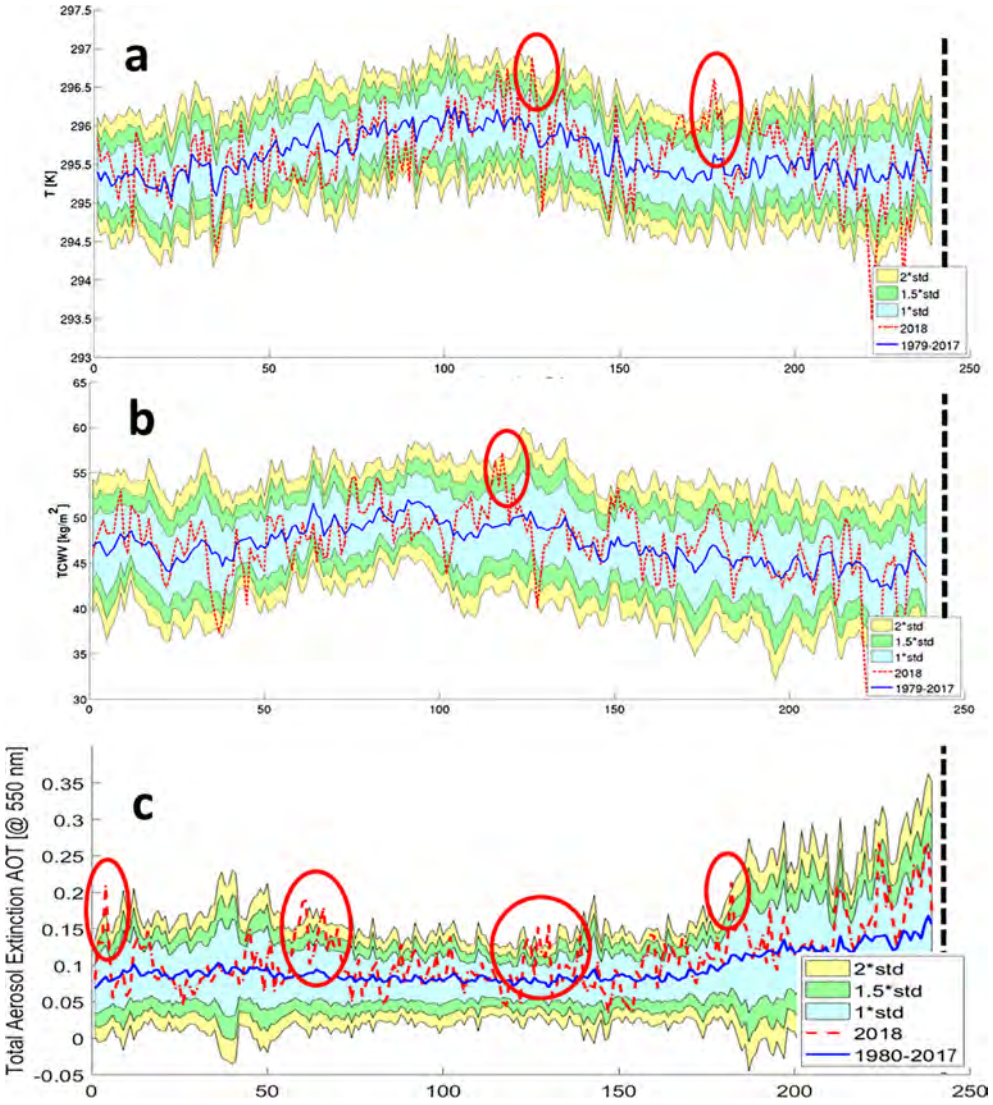

Fig. 3. Climatological analysis performed from February 2nd, 2018 until the day of the Indonesian earthquake (September 28th, 2018) (the last day of each time series is the day before the earthquake) for (a) skt, (b) tcwv and (c) AOT. The x-axis indicates the number of days after February 2nd, 2018. Blue line represents the historical mean and cyan, green and yellow bands represent 1.0, 1.5 and 2.0 standard deviations, respectively. The red dashed line represents the value of the specific parameter in the earthquake year (i.e. 2018). The day of the earthquake is represented as a vertical black dashed line. (For interpretation of the references to colour in this figure legend, the reader is referred to the web version of this article.)

as the "crests" of the EIA. Such phenomenon is due to the mutual interaction between electric and geomagnetic field (**ExB**) that moves the ionospheric plasma in the upward direction at the magnetic equator. Pressure gradient and gravity result into the down lift of the plasma along the magnetic field lines increasing the vertical integrated electron density over the region at ± 15/20 geomagnetic latitude degrees. It could appear rarely even in night-time, but during high solar activity (e.g. Walker et al., 1994; Chen et al., 2008), which is not in the year of this study (2018 is practically a minimum of solar activity). Past different studies proposed an increase of the ionization of the crests of EIA or their appearance during night-time as a phenomenon possibly induced by earthquakes (e.g. Parrot, 2013; Kuo et al., 2014, Oikonomou et al., 2016). Therefore, we need to define an electron density background before searching for a possible positive increase. To this scope, we use two kinds of background: first, we use the International Ionospheric Model IRI – 2016 (Bilitza et al., 2017) and, second, we construct a background with the same CSES satellite data for a period of about three non-consecutive months.

The first background is calculated using the IRI Model – in a small cell of 6° longitude × 4° latitude (117°E ≤ long. ≤ 123°E and 2°S ≤ lat. ≤ 2°N) at the altitude of the CSES satellite for the two local times of CSES (about 2 LT for night and about 14 LT for day) with a time resolution of one day. Fig. 4 shows the histogram of the distribution of the percentage differences between the CSES Ne and the values estimated by the model computed at the same satellite altitude in the same days. In this area, the CSES electron density is much lower than IRI values by about 60%, and, for this reason, normally the IRI is not a reliable background to search for possible seismo-induced disturbances in the ionosphere.

Therefore, to estimate night-time and day-time backgrounds, we fully resorted to the available CSES data. The Sun-synchronous orbit of CSES simplifies this task as the local time is fixed during night-time and day-time at about 02 and 14 LT, respectively.

The background is estimated in mid-latitude and equatorial regions, i.e. inside |geographical latitude| ≤50°. We estimated the background only under quiet geomagnetic conditions, to exclude the possible effect of the external forcing. The quiet geomagnetic conditions are defined according to the investigated latitudinal region. All the background analyses are performed under G0 geomagnetic activity (ap ≤ 32 nT) in the previous 24 h. For equatorial region (|lat| < 35°), we applied more restricted conditions: we also take into account the Dst (Disturbance Storm Index) as it is an indicator of the geomagnetic activity at the equator, considering |Dst| ≤ 20 nT during satellite acquisition time and |Dst| ≤ 30 nT in the previous 24 h. The geomagnetic indices data have been downloaded from http://wdc.kugi.kyoto-u.ac.jp/dstae/index.html. The investigated region is divided into cells of 5° longitude × 5° latitude. Each cell must contain at least ten samples to define a background median value. The tracks that present negative values of

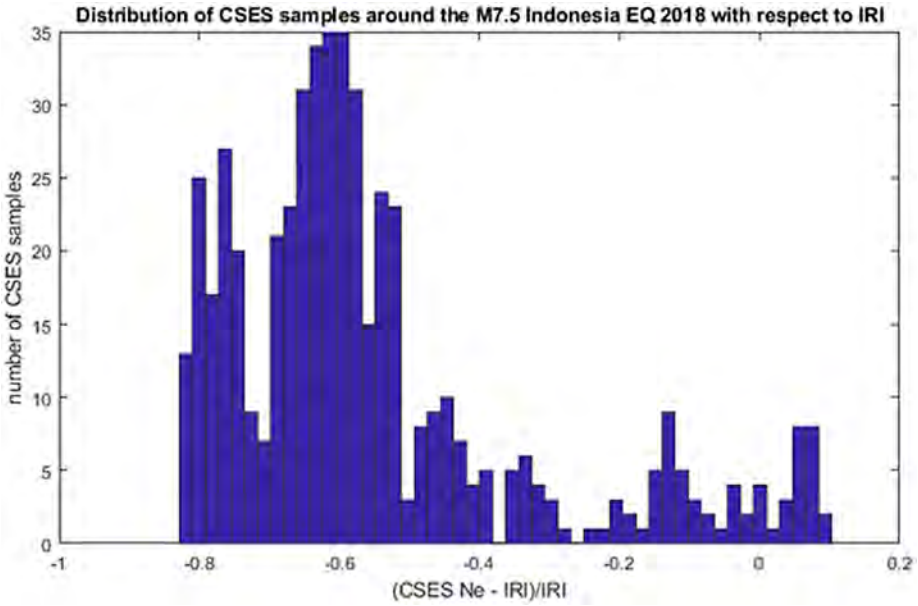

Fig. 4. Comparison of electron density measured by LAP onboard CSES with respect to IRI-2016 inside a box with 117° E ≤ long. ≤ 123°E and 2°S ≤ lat. ≤ 2°N.

electron density (i.e. without physical meaning) are excluded from the estimation of this background to avoid wrong values due to satellite (or data processing) technical problems.

Figs. 5 and 6 present the estimated electron density background for night-time and day-time, respectively. The white cells are due to lack of data or insufficient number of samples in quiet geomagnetic conditions (as defined above).

Some statistical parameters are reported in Table 2, providing an evaluation of the computed backgrounds. The standard deviation σ_b is the total standard deviation computed over each median value of each cell, as well as the bias is the sum of the deviations of each Ne sample and its cell Ne median value with respect to the Ne samples as given by the following equations:

$$\sigma_b = \sqrt{\frac{\sum_p \sum_{i=1}^{n} (Ne_i - M\_Ne_p)^2}{N-1}} \tag{3}$$

$$bias = \frac{\sum_p \sum_{i=1}^{n} \frac{Ne_i - M\_Ne_p}{Ne_i}}{N} \tag{4}$$

where Ne_i is the electron density of the i-th sample inside the p-th cell, characterized by its median value M_Ne_p and N is the total number of considered samples.

As we expected, the night-time background is more stable than day-time one. Instead, the day-time background median values are closer to the specific values (the Mean Relative Deviation and bias are lower, see Table 2 for more details).

We also computed a second background for each month of the available data, i.e. April, August and September 2018. By dividing the

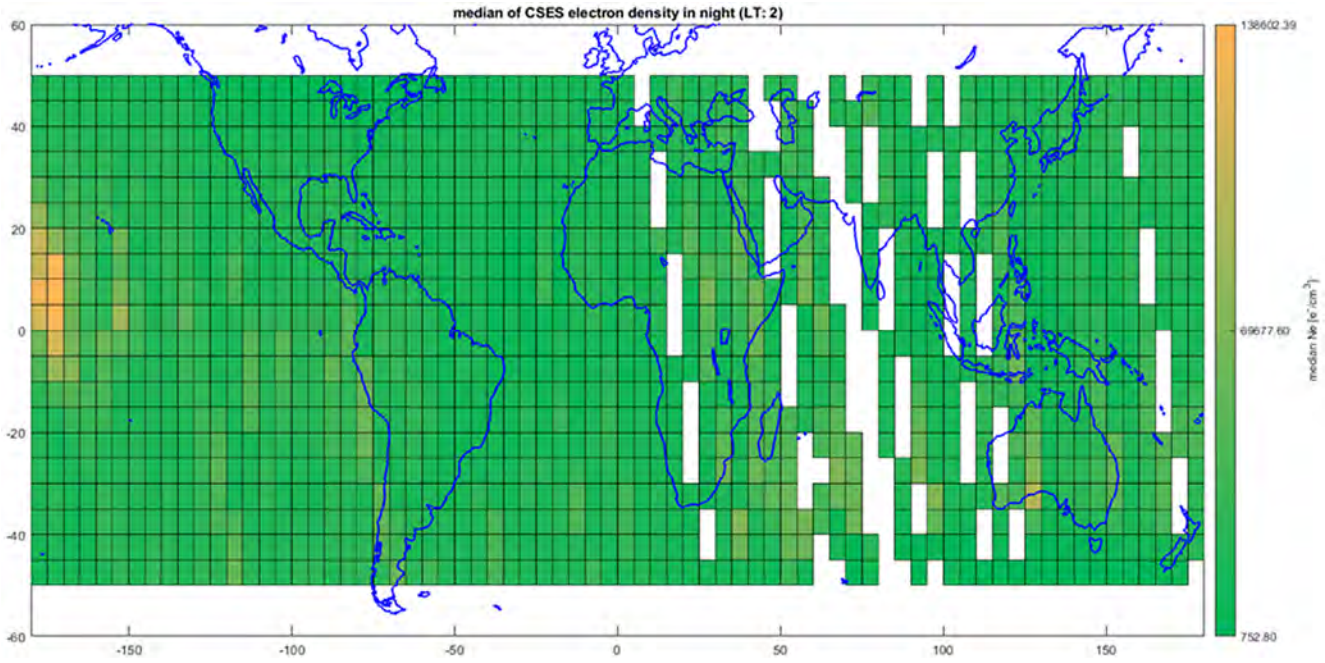

Fig. 5. CSES night-time (02LT) electron density background characterization.

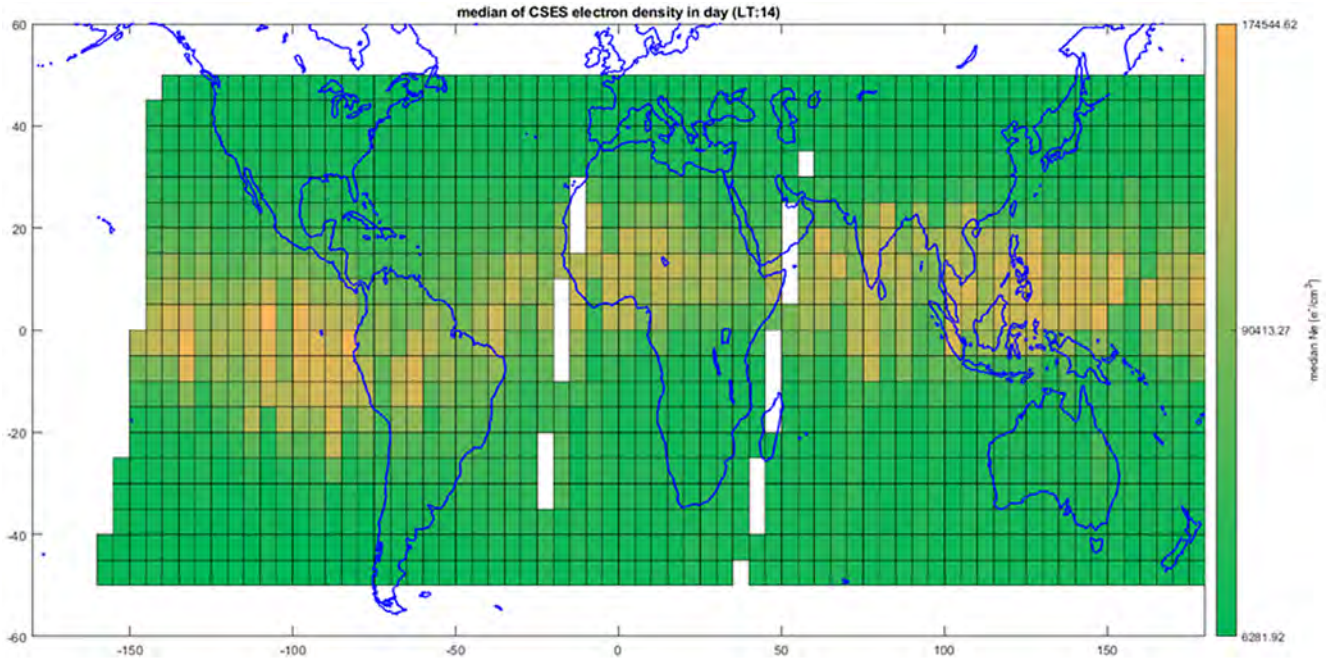

Fig. 6. CSES day-time (14LT) electron density background characterization.

Table 2
Statistical evaluation of the night-time and day-time CSES backgrounds.

	Night-time	Day-time
Standard deviation σ_b	$1.78 \cdot 10^4\, e^-/cm^3$	$2.30 \cdot 10^4\, e^-/cm^3$
Mean Relative Deviation (MRD)	44.1%	31.0%
Bias	−12.6%	−7.68%
Number of used samples	164,223	173,225

months, it is possible to reduce the effects due to the well-known seasonal variation of the electron density in the ionosphere.

With the monthly characterization, we search for the positive anomalous samples inside Dobrovolsky's area as the samples that deviate more than 30% with respect to the median value of the corresponding cell. Table 3 reports the results of this analysis for April, August and September 2018. We take into account only the data that preceded the mainshock. We search for the positive anomaly to look for an enhancement of the electron content in ionosphere possibly due to the preparation of the impending earthquake. In April, we identify 116 positive anomalous samples inside Dobrovolsky's area in night and day time with respect to 1258 samples in the same area and period, so the 9.22% are 30% positively higher than the Ne median value. In August we detected 930 anomalous samples over 5476, so 16.98% and finally in September 614 anomalous samples over 4097, so 14.99%.

It is interesting to note that in the two months before the occurrence of the earthquake the percentages of the positive anomalous samples are higher than those in April 2018. In the same two months, we also detect a seismic activation of the region (see Section 3.1). The analysis is promising, but to confirm a possible link between these anomalies and the earthquakes more complete data are necessary. A further improvement of this work could be carried out with the future releases of CSES data.

3.4. Electron density anomalous signals from CSES satellites

All the available CSES plasma tracks crossing Dobrovolsky's area before the Mw = 7.5 Indonesia 2018 earthquake have been processed. For each track, a graph has been produced with the absolute values of electron density, electron temperature, and an automatic analysis of their residuals with respect to a cubic spline and their temporal (and spatial) derivative. The unpredictable presence of spikes suggested us to make a visual inspection track by track. With this operation, we can identify the tracks acquired during G0 geomagnetic conditions ($ap \leq 32$ nT) that present some particular features, i.e. some significant signal in the residual analysis and we manually classify this track as anomalous. Table 4 lists the CSES-Ne tracks identified as anomalous. In supplementary material, we provide the corresponding figure for each track listed in Table 4. No daytime CSES track presents significant features. Two of the selected tracks acquired on August 18th, 2018 and August 20th, 2018 present a low-moderate geomagnetic activity.

By comparing Tables 1 and 4, i.e. the occurrence of the anomalies with the earthquakes sequence, it is possible to note that most of the ionospheric anomalies are followed within some days with at least an earthquake in the area. Despite the limited availability of satellite tracks, we tried to perform a preliminary statistical verification of this characteristic. Table 5 is the corresponding error matrix that resumes the classification of the Ne satellite tracks, showing if they present a clear anomaly in Ne latitudinal profiles and if they precede by no more than 10 days an M5.5 + earthquake in the investigated area, at maximum depth of 50 km. Only the tracks in geomagnetic quiet time

Table 3
Number of positive anomalous CSES Ne values (i.e. greater than 30%) with respect to the CSES Ne background. Only geomagnetic quiet time as described in the text was investigated inside the Dobrovolsky's area (indicated below as Dob.).

Investigated month	April 2018	August 2018	September 2018
Number of anomalous Ne values inside Dob.	116	930	614
Number of investigated values inside Dob.	1258	5476	4097
Percentage of anomalous samples	9.22%	16.98%	14.99%

Table 4
List of the CSES-Ne tracks identified as anomalous.

Date	Time (UT)	Geomagnetic conditions	Geom. Latitude (°)	Anomaly width (°)	Night / day	Notes
2018–04-07	17:39	Dst = 11 nT, a_p = 5 nT	−13	3	Night	The general profile is a bit irregular
2018–08-02	18:31	Dst = 6 nT, a_p = 2 nT	−10	10	Night	The same day is detected anomalous on Swarm
2018–08-04	17:53	Dst = −5 nT, a_p = 3 nT	−8, −4	1 × 2	Night	
2018–08-06	17:15	Dst = 4 nT, a_p = 2 nT	−8	6	Night	Clear anomaly
2018–08-08	18:12	Dst = −6 nT, a_p = 4 nT			Night	EIA profile in night track (LT = 02:01)
2018–08-17	18:31	Dst = −18 nT, a_p = 2 nT	5	10	Night	The anomaly is partially outside Dobrovolsky
2018–08-18	18:12	Dst = −26 nT, a_p = 9 nT	−17	2	Night	
2018–08-19	17:54	Dst = 11 nT, a_p = 7 nT	−7	3	Night	There are two peaks almost symmetric with respect to magnetic equator (see discussion in Sec. 3.6)
2018–08-20	17:34	Dst = −20 nT, a_p = 15 nT	−8	10	Night	There are three peaks in 10 lat. degrees with some irregularities inside
2018–09-03	17:53	Dst = 1 nT, a_p = 4 nT	2	4 anomalies of about 2°	Night	The overall length covered by the anomalies is about 10° all inside Dobrovolsky's area
2018–09-07	18:11	Dst = −6 nT, a_p = 4 nT	0, −5	1	Night	One signature could be due to the equatorial electroject, but there is also another peak of Ne at −5°

Table 5
Error matrix of the available CSES Ne tracks in geomagnetic quiet time with the earthquake occurrence. The earthquakes are selected in the investigated area, max 50 km depth, M5.5+, in the next 10 days after the Ne anomaly.

Total cases 45		Earthquake	
		Yes	No
Ne CSES anomaly	Yes	20	1
	No	16	8

(|Dst| ≤ 20 nT and a_p ≤ 10 nT) have been taken into account. In the main diagonal of the error matrix, there are the "good cases", i.e. the anomaly was followed by an earthquake or absence of anomaly in period without earthquakes. The other two cells represent the false alarms, i.e. the anomaly is not followed by a seismic event, or quiet tracks were followed by a seismic event. Based on Table 5, it is possible to calculate some statistical parameters as the accuracy, the false alarm rate and the hit rate (e.g. Fawcett, 2006), as defined by the following equations:

$$Acc = \frac{\sum (yes\ \ anom.\ yes\ \ EQ) + \sum (no\ \ anom.\ ,no\ \ EQ)}{N},$$

$$FA = \frac{\sum (yes\ \ anom.\ ,no\ \ EQ)}{\sum (noEQ)},$$

$$HR = \frac{\sum (yes\ \ anom.\ ,yes\ \ EQ)}{\sum (EQ)}$$

where N is the total number of case studies (in our case 45), and $\sum(\cdots,\cdots)$ is the sum of number of cases selected according to the indication in brackets. For our statistical analysis, we obtain an accuracy of 66.2%, a false alarm rate of 11.1% and a hit rate of 55.6%. As the accuracy is higher than 50%, we can consider that the hypothesis is confirmed. Nevertheless, many more satellite data and a longer time interval are needed to confirm better this kind of correlation.

3.5. Magnetic observations from CSES data

In this section, we present a preliminary analysis of the magnetic field measurement acquired by High Precision Magnetometer FGM1 onboard CSES. Due to lack of data quality in the present release, we reserve the possibility to repeat this analysis with future data releases.

The applied method is very similar to the one successfully applied to Swarm magnetic data investigating various earthquakes in the world: Mw = 7.8 Nepal 2015, Mw = 7.8 Ecuador 2016, Mw = 6.5 Italy 2016, Mw = 8.2 Mexico 2018, Mw = 7.3 Iran 2018 earthquakes (De Santis et al., 2017, Akhoondzadeh et al., 2018, Marchetti et al., 2019a, Marchetti and Akhoondzadeh, 2018; Akhoondzadeh, 2019, respectively). Firstly, a numerical approximation of the time derivative is estimated by the first differences divided for the time difference of two consecutive samples. Secondly, a cubic spline is fitted over the data, and the residual is analysed and plotted.

Fig. 7 presents the HPM data analysis applied to the track of the orbit 2934 acquired on August 14th, 2018, at 6:02 UTC above the Dobrovolsky's area. In the supplementary material other two tracks are shown as acquired on August 4th and 9th 2018, respectively (Figs. S11 and S12). All the investigated tracks present some little spikes due to little jumps of the order of 10–100 nT in original data transformed in spikes by the derivative operation. We do not know the reason and/or the source (instrumental or raw data processing) of these jumps, but we exclude that they are real characteristics of the ionospheric magnetic field. Despite this, we notice in the track of Fig. 7 an anomalous signal at the same latitude of the future epicentre that could be a possible candidate for a seismically induced phenomenon. All the reported tracks were acquired in quiet geomagnetic conditions as testified from the geomagnetic indices Dst and ap reported on the figure headings.

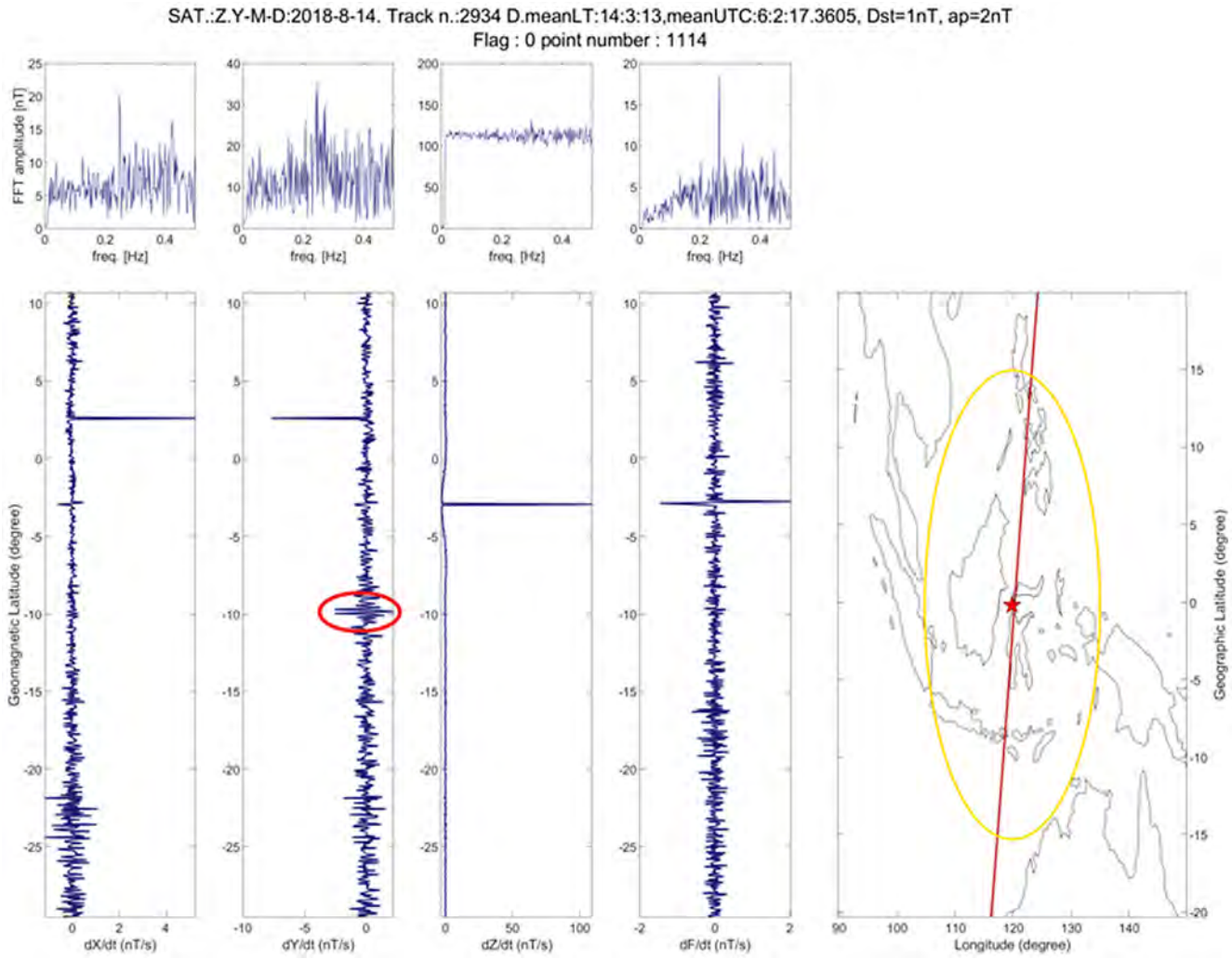

Fig. 7. CSES HPM track crossing the Dobrovolsky's area and future Mw7.5 Indonesia epicenter on August 14th, 2018. The red circle underlines an anomaly in East-Y component of magnetic field. The map at the right presents the projection of the CSES track on ground with a brown line, the epicenter by a red star and the Dobrovolsky's area by a yellow circle. (For interpretation of the references to colour in this figure legend, the reader is referred to the web version of this article.)

This condition permits to exclude a solar ionospheric disturbance. In the supplementary material the two tracks are reported at the same longitude in two different days, the one acquired on August 9th, 2018 does not present any anomaly similar to the one of the 14th, otherwise the track acquired on August 4th 2018 presents an anomaly but it is located southern the future epicentre, although completely inside the Dobrovolsky's area. This track could be considered as a candidate for seismo-induced phenomena.

A new release and wider data availability of CSES could permit in future to better discriminate between the more reliable seismic induced anomaly and other source of anomalies.

3.6. Electron density anomalies on night-time of August 19th, 2018 over the epicentral area

Checking the electron density profiles acquired over the area by Swarm and CSES satellites, we notice the presence of small peaks of electron density during night time (02:01 and 03:10 LT, for CSES and Swarm satellites, respectively) over the epicentral area on August 19th, 2018. Fig. 8 shows the electron density latitudinal profiles acquired on August 19th, 2018 over and around epicentral area by Swarm Alpha, Bravo and Charlie and CSES satellites during night time. Panels (a), (c) and (d) represent Charlie Ne acquired at about 3:10 LT in left side, over and right side with respect to the epicentral area, respectively; panel (b) represents a track of Alpha acquired on epicentral area about 6 s after the close Charlie pass. Maps of the area with ground projection of satellite tracks are represented in panels (e) and (l). The satellite name, direction (U for Upward, D for Downward) and UT time at track center are labeled for each track. Panels (f) and (g) represent the Ne profiles acquired by CSES in left side and over epicentral area, respectively. Panels (h) and (i) show the Ne profiles acquired by Swarm Bravo in the same area but some hours before. The figure represents in the upper part the electron density profiles of Swarm Alpha and Charlie satellites and in the lower part the CSES and Swarm Bravo satellites. In this way, the altitude of each part is comparable, as Swarm Alpha and Charlie fly at about 445 km altitude, Swarm Bravo at about 510 km and CSES at about 505 km. The local time of the upper panel is between 3:04 and 3:10, CSES satellites crossed the area about one hour before at 02:02 LT and Bravo even some hours before at 22:03 of the previous day. Despite the different local times, it is evident that the absolute value of CSES electron density is much less than the Swarm measurements. However, since the goal of this part is to investigate the anomalous variations of the electron density, this mismatch does not affect meaningfully our analysis. The most striking feature is the panel (c) of Fig. 8 that shows the presence of two electron density peaks underlined by red circles. It is noticeable that the peaks are almost symmetric with respect to the geomagnetic equator and covering a very narrow latitudinal sector. This suggests that the mechanism ruling out the appearance of such

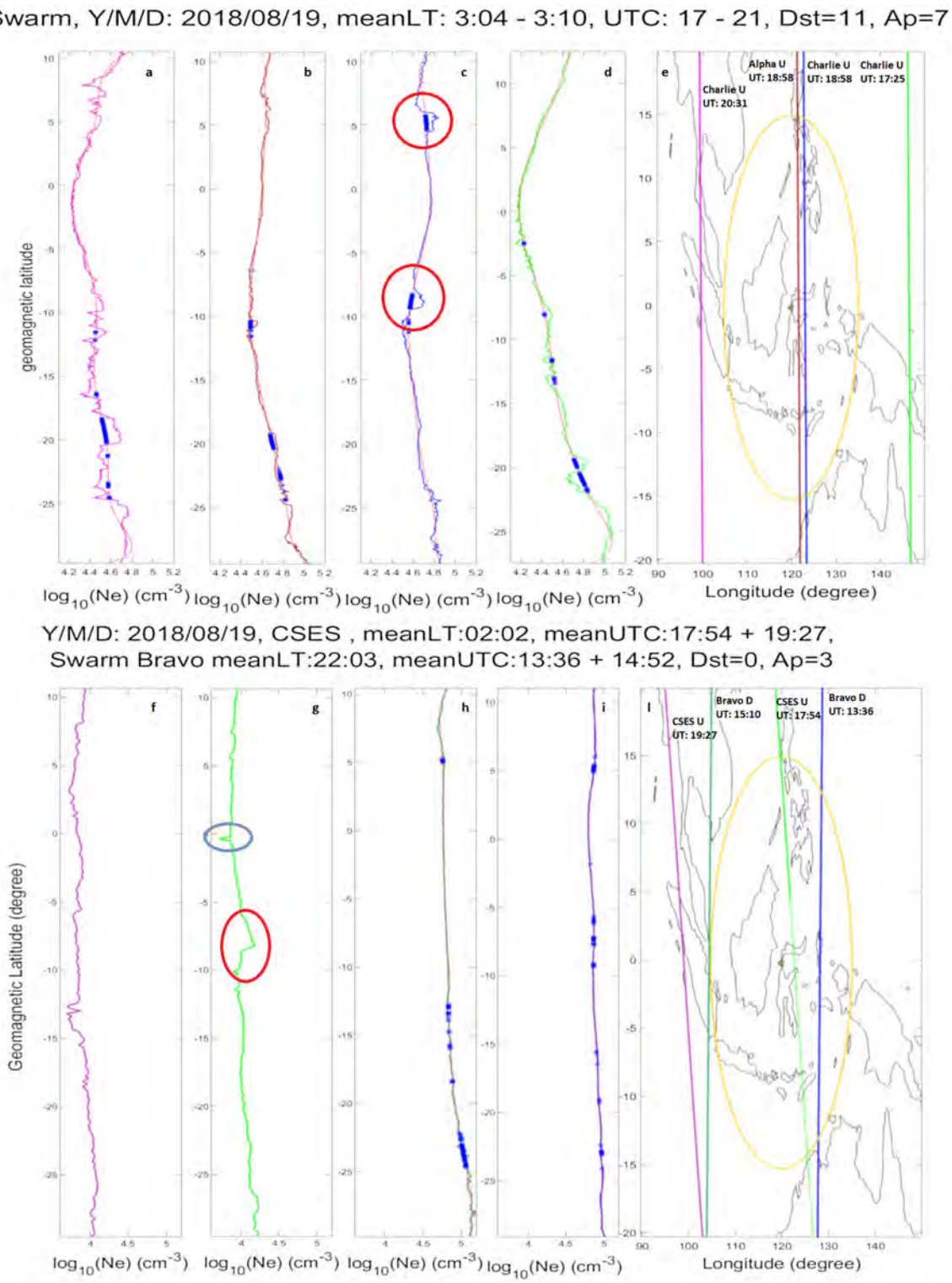

Fig. 8. Electron density profiles acquired on August 19th, 2018 over and around epicentral area by Swarm Alpha, Bravo and Charlie and CSES satellites during night time. (a), (c) and (d) represent Charlie Ne acquired at 3:10 LT in left side, over and right side with respect to the epicentral area respectivetely. (b) represents a track of Alpha acquired on epicentral area about 6 s after the close Charlie track. Maps of the area with ground projection of the satellite tracks are represented in panels (e) and (l). The satellite name, direction (U for Upward, D for Downward) and UT time at track center are labeled for each track. (f) and (g) represent the Ne profiles acquired by CSES in left side and over epicentral area, respectivetely. (h) and (i) show the Ne profiles acquired by Swarm Bravo in the same area but some hours before.

peaks may be a local flip of the **E** field at the dip equator from westward to eastward and consequent variation of the intensity and direction of the EEJ resulting into a uplift of the ionospheric plasma reaching the Swarm altitudes. In the previous track (d) and the next track (a) this feature is not present, although they are acquired at the same local time. The track of Alpha (b), that crossed the same area about 6 s after, shows a similar signature of the peaks, even if with a significantly lower intensity, suggesting that the found phenomenon could be rapid (i.e.

changes in the scale of some seconds) or very localized geographically as there is a difference of about 1.4° in longitude between Alpha and Charlie satellites. This suggests that such feature is found in a very narrow longitudinal sector, covering the epicentral area.

Now we study CSES electron density profile acquired in the area (g) about one hour before. We do not investigate deeply the quick change over the geomagnetic equator: difficult to say whether it is real or a instrumental artifact. On the other hand, an enhancement at about −8° geomagnetic latitude is found, as underlined by the red circle. This seems to be related to the south peak found by Swarm Charlie, even if it covers a wider latitudinal sector. No appearance of a northern peak, as detected by Charlie satellite, is found by CSES. This may be explained by the fact that CSES orbit is more inclined with respect to Swarm orbits. Thus, the northern part of the orbit is closer to Alpha longitude and does not show a clear electron density peak, which is in agreement with the measurements of Swarm Alpha. Conversely, the southern part of the CSES orbit is closer to the Charlie orbit, and it shows the southern peak (red circle in (g)). By the comparison of Swarm and CSES Ne measurements, it is possible to conclude that the found electron density enhancement is in both satellites of the same order (i.e. 10–20 $10^3\,cm^{-3}$) and occurred at a very narrow longitudinal sector (about 123° East) during night-time (at least between 02 and 03 of the night).

Regarding the possible nature of such peaks as due to geospace forcing, despite the geomagnetic conditions were low ($|Dst| < 20$), the Interplanetary Magnetic Field (IMF) was charaterized by a turning from southward to northward between 17:00 and 18:00 UTC (not shown). The z-component of the IMF (IMF-Bz) remained to northward conditions until 21:00 UTC and reached values up to about 8 nT (not shown). In correspondence, an increase of the auroral activity is found, with AE index reaching 500 nT right before 18:00 UTC (not shown). This leads to overshielding conditions due to the relative intensities of the Region 1 (R1) and Region 2 (R2) field-aligned currents (FACs) resulting into a penetration of electric fields of magnetospheric origin into low-latitudes through the Earth-ionosphere waveguide (Abdu et al., 2009; Wei et al., 2015; Fejer et al., 2017). The overshielding conditions lead to perturbations of the electric field that are dusk-to-dawn, i.e. westward in the dayside and eastward in the nightside (see, e.g., Venkatesh et al., 2017 and references therein). In our case, the geospace conditions may support a reversal of the night-time westward EEJ into an eastward EEJ of sufficient entity to produce the found peaks. However, some outstanding issues remain. First of all, the narrow longitudinal sector in which the effect is confined may suggest a very peculiar zonal effects. In addition, to confirm the geospatial origin of the found electron density peaks, companion measurements must be added. However, as reported in Spogli et al. (2016) and Povero et al. (2017), the South-East Asia region is not covered by magnetometers (for the EEJ intensity and direction estimation) or ionosonde (for the determination of the bottomside ionospheric uplift) located at the dip-equator. Also measurements from incoherent scattering radars able to provide altitude variations of the electron density are missing in the region. Thus, a final word cannot be told about the internal or external origin of such disturbance.

Concerning possible connection with seismic activity, in the same day some significative earthquakes occurred in the Dobrovolsky's area (see Table 1). All the phenomena occurred in the same fault, and their localisation is approximatively: 8.3° lat. S, 116.6° long. E and they occurred between 4:10 UT and 15:28 UT. The major event was an earthquake with magnitude Mw6.9 occurred at 14:56. The electron density enhancement was recorded about from 3 to 4 h after that major event and 2.5 h after the last seismic M5.5 + event of the same day in the Dobrovolsky's area. We consider this time too long to hypotise a co-seismic impact in the ionosphere by gravity waves induced by these events that is, otherwise, typical of some decades of minutes (see e.g. Jin, 2018). In addition, an effect triggered by gravity waves would have appeared as a planar wave from the epicentre, that it is not the case here highlighted. Thus, by excluding co-seismic effects of the activity for this day and by not being able to completely determine the triggering due to external origin, we suggest that this phenomenon could be related to the preparation of the Mw7.5 Indonesia earthquake, although the seismic events that preceded this phenomenon could have played some role, for example, pushing some gas/fluid out from the other fault responsible for the main event.

Therefore, we may consider this phenomenon as likely related to the preparatory phase of the Mw = 7.5 Indonesia 2018 earthquake, following what proposed by other authors in a dedicated LAIC simulation to correlate variations of the low-latitude ionosphere electrodynamics following the accumulation of charge carriers over the Earth's surface (e.g. Kuo et al. 2014). In the Discussion we propose a simple explanation of the possible phenomenon.

3.7. Magnetic field investigation on the epicentral area by Swarm constellation

The absolute scalar intensity of magnetic field during geomagnetic quiet time ($|Dst| \leq 20$ nT and $a_p \leq 10$ nT) from Swarm satellites has been analysed to detect variations before the earthquake occurrence. To achieve this objective, it is necessary to remove a geomagnetic model of the field. This is important to take into account that the satellite measurements could be taken at a different altitude. For Swarm constellation we will consider two different altitudes, i.e. one lower altitude for Alpha and Charlie and another higher altitude for Bravo. There exist different models of the geomagnetic field: International Geomagnetic Reference Field (IGRF), CHAOS, World Magnetic Model (WMM), etc. The differences between the models depend on which sources and variability they consider. Here we use the IGRF-12 (Thébault et al., 2015) that estimates only the contribution of the main field from the Earth core, which it is adequate for our purpose. As the lithospheric field and external field are not modelled, there will be a residual value, that, together with eventual oscillations, will be removed by further data processing. The model is calculated for each sample to take into account the slightly different altitude of the satellite mainly due to the small ellipticity of the orbit.

A third degree polynomial has been further removed to mitigate possible seasonal variations after model subtraction. Fig. 9 shows the residual of the analysis of Swarm magnetic field intensity. The analysis underlines four anomalous days: three are negative, i.e. a decrease of intensity of the magnetic field on March 3rd, May 13th and on September 27th while the one on August 2nd is positive. The decrease of geomagnetic field recorded on May 13th is probably due to the recovery phase a geomagnetic storm occurred on May 6th, 2018. For this reason, we exclude this anomaly as a possible pre-seismic candidate (shown as a red cross on the graph). We note that the last negative anomaly occurred the day before the earthquake. The positive anomaly of August 2nd occurred in quiet geomagnetic time and on the same day we detected an anomaly in Aerosol Optical Thickness in the atmosphere.

The same procedure has been applied to the Y (East component) of the geomagnetic field. Among the three components of the geomagnetic field we selected this one because it is the most promising for internal sources anomalies (Pinheiro et al., 2011) and, from previous works on other earthquakes (De Santis et al., 2017, Akhoondzadeh et al., 2018, Marchetti et al., 2019a,b), it seems more sensitive to a possible lithospheric activity. Fig. 10 presents the result of the analysis of Swarm Y magnetic component from February 1st, 2018 to the September 27th, 2018 (i.e. the day before the Mw7.5 Indonesia earthquake) following a similar approach to that used with the intensity. Considering a threshold of 1.25 times the interquartile, it is possible to extract 14 anomalous days, ten positive and four negatives. We do not consider as possible candidates of seismic precursors the anomalies on May 13th, 2018 (the same day of F analysis) and on August 16th, 2018, both occurred just after some solar geomagnetic activity. It is interesting to note the group of anomalies near or on adjacent days from July, 31th to August 5th, 2018. This latter period is the same found as anomalous by

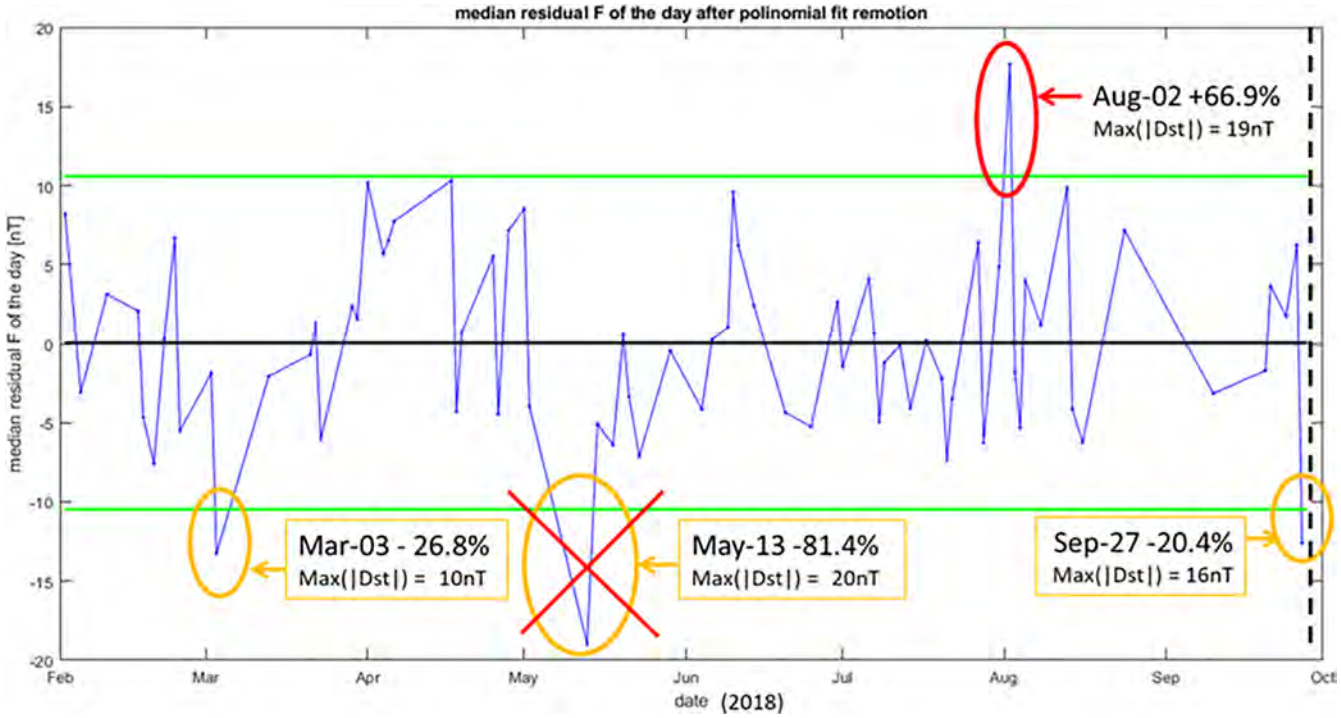

Fig. 9. Swarm residual of magnetic field intensity F over Indonesia from 1st February 2018 until the Mw7.5 Indonesia September 28th, 2018 earthquake (not included). The green horizontal lines represent the median plus or minus 1.25 times the interquartile, so about 2 standard deviations and they are the selected thresholds to detect anomalies following Akhoondzadeh et al. (2018, 2019). The vertical black dashed line shows the day of the occurrence of the earthquake. Red circle underlines a positive anomaly and yellow circles the negative ones. The cross over the anomaly is due to the exclusion of possible seismic relationship (see text for discussion). The anomalies are labeled with the day of occurrence, the percentage of the anomaly over the median and the maximum absolute daily value of Dst. (For interpretation of the references to colour in this figure legend, the reader is referred to the web version of this article.)

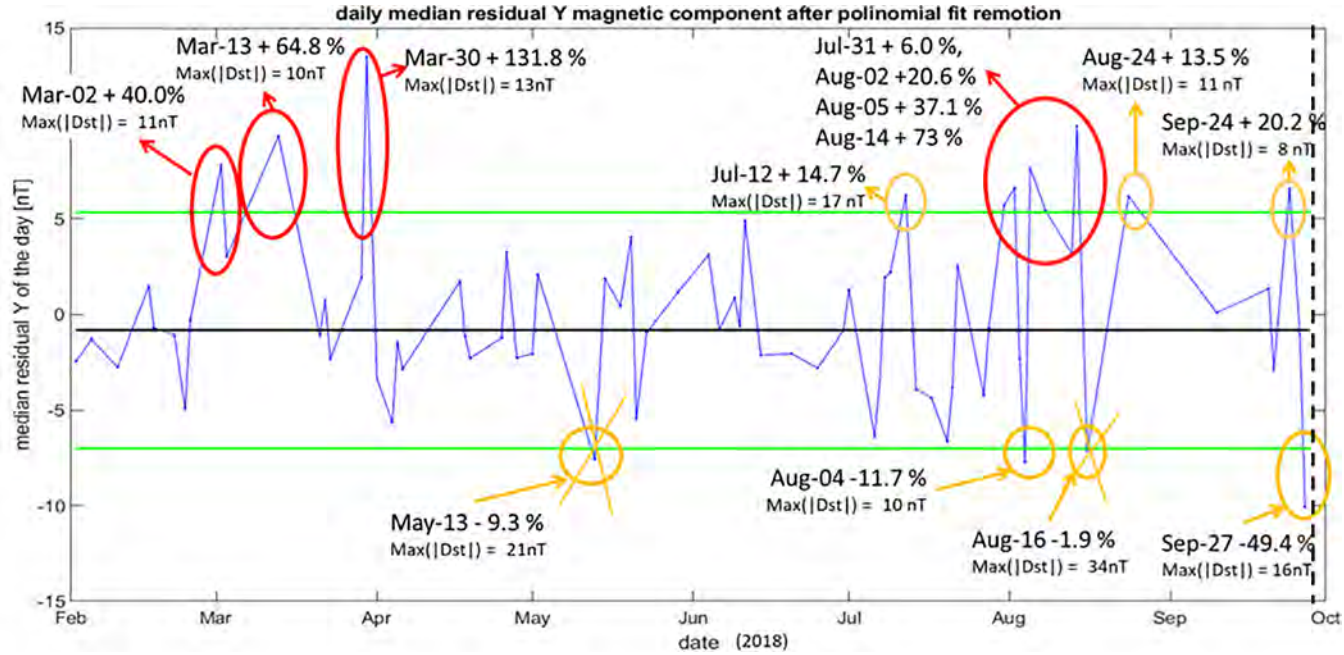

Fig. 10. Swarm residual of magnetic Y component over Indonesia from February 1st, 2018 until the Mw7.5 Indonesia September 28th, 2018 earthquake (not included). The green lines represent the median plus or minus 1.25 times the interquartile and they are the selected thresholds to detect anomalies. The vertical black dashed line shows the day of the occurrence of the earthquake. Red circles highlight the positive anomalies and yellow circles the negative ones. The cross over some anomalies means the exclusion of possible seismic relationship (see text for discussion). The anomalies are labeled with the day of occurrence, the percentage of the anomaly over the median and the maximum absolute daily value of Dst. (For interpretation of the references to colour in this figure legend, the reader is referred to the web version of this article.)

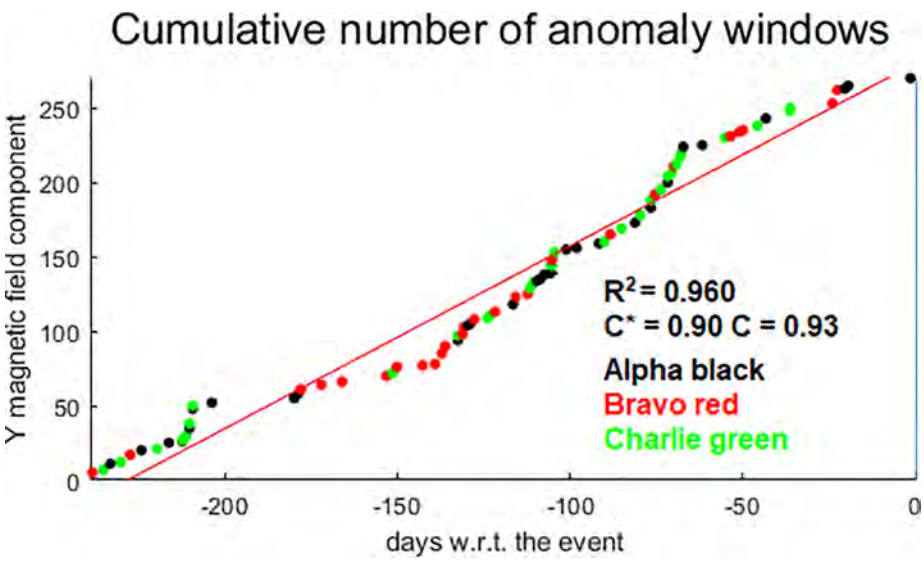

Fig. 11. Cumulative number of Swarm anomalies automatically detected in the residual of magnetic Y component in the Dobrovolsky's area from February 1st, 2018 until the Mw7.5 Indonesia September 28th, 2018 earthquake, only during quiet magnetic times. The colour of the dot represents the satellite that detects the anomaly: black for Alpha, red for Bravo and green for Charlie. (For interpretation of the references to colour in this figure legend, the reader is referred to the web version of this article.)

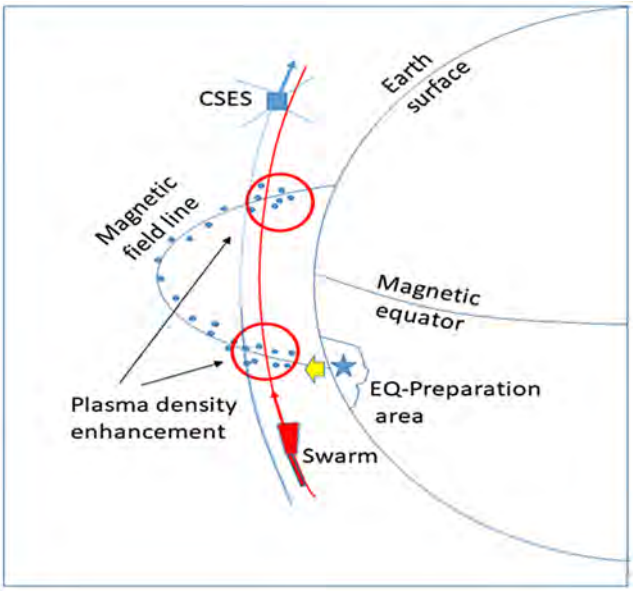

Fig. 12. Possible scheme of the potential precursory phenomenon above the epicentral region. An upward electric charges flux from the earthquake preparation area along the magnetic field line produces the corresponding plasma enhancement just above the epicentral region and its conjugate point. The star represents the impending earthquake hypocentre. The picture is not to scale.

the total intensity, F, analysis of Swarm geomagnetic field and by atmospheric analysis.

Both previous analyses of the Swarm geomagnetic field are based on the check of the daily value of some quantity compared with the typical value for that area extracted by time series. That type of analysis assumes implicitly that the possible seismic effect persists in the ionosphere for at least one day. As in the past also some rapid electromagnetic emissions were recorded, we decided to apply a second technique, based on the analysis of the residual of the derivative of the Y component of the geomagnetic field along the track and the subtraction of a cubic-spline (details of the method in De Santis et al., 2017). The residual is analysed by 3-degree latitude moving windows estimating the root mean square rms inside the window and comparing this value with the Root Mean Square RMS along the whole track inside +/− 50 geomagnetic latitude degrees. If the rms in the windows is higher than two times the RMS of the track and the geomagnetic conditions are quiet ($|Dst| \leq 20$ nT and $a_p \leq 10$ nT), we define that window as anomalous. Fig. 11 shows the cumulative number of the anomalous windows from February 1st, 2018 until the mainshock occurrence. As also without earthquake we expect some anomalies due to other factors, we search for possible deviation from linearity that here is fitted by a red line. The overall coefficient of determination of the linear fit is $R^2 = 0.960$ that is less than 0.970 that is the threshold that was used in other works (Akhoondzadeh et al., 2018, Marchetti et Akhoondzadeh, 2018; Akhoondzadeh et al., 2019) to classify this analysis as positive. Another statistical parameter is the C* (and C) that is the ratio between the anomalies of Bravo (the highest satellite) with respect to the half of the anomalies of Alpha and Charlie (the lowest ones). The parameter C without asterisk is normalized with respect to the number of windows of each satellite that are inside the Dobrovolsky's area in quiet geomagnetic times (so the ones that potentially could be anomalous). For anomalies that come from lithosphere, we expect to find more of them in the lowest satellites, so we consider positive this analysis when this parameter is less than unity. This analysis passes both criteria, so we can define it as successful.

By visual inspecting of the cumulate (Fig. 11), we note an increase of the anomalies around February 25th, 2018 and a second increase or acceleration from July 10th to July 20th, 2018. In particular, the second one seems interesting as it is distributed on a longer period with data continuity.

4. Discussion

By investigating the USGS earthquake catalog in the year before the mainshock, we find from two months before the Mw7.5 September 28th, 2018 Indonesia earthquake, that the region inside the Dobrovolsky's area shows a seismic activation of the shallow lithosphere, with a final seismic acceleration in the very last days.

The atmosphere presents some anomalies mainly in Aerosol Optical Thickness, and a few others in skin temperature and water vapor.

The ionosphere presents most of the disturbances during the month of August 2018. The presence at the end of August of a geomagnetic storm and other global geomagnetic events are avoided in this study excluding the time when the geomagnetic indices Dst and a_p exceed

pre-chosen thresholds.

The Swarm magnetic field acquired on August 2nd, 2018 presents an anomaly and at the same time, the atmosphere shows a disturbance in aerosol content, which represents the spatially closest anomaly to the impending earthquake epicentre (see Movie in the supplementary material). The same day (i.e. August 2nd, 2018) the electron density acquired by CSES satellite presents an anomaly. This gives a good idea about the reliability of CSES electron density data for this scientific purpose and it supports that the anomaly is real and not due to instrument malfunction or data processing (totally different for these analyses).

In addition, on August 19th, 2018 we detected the presence of enhancements of the in situ electron density at the Swarm and CSES altitudes and symmetrically with respect to the dip equator during night time (about from 02 to 03 LT), not present in the nearest area outside Dobrovolsky's region at the same time. We also discussed the geospace conditions to check for the possible external origin of such phenomenon, without finding a strong argument to completely support the triggering of such phenomenon from EEJ disturbance following the prompt penetration of electric field from auroral latitudes. We cannot exclude that its presence could be due to the preparation of the earthquake, as also found in the simulations shown by Kuo et al. (2014). Fig. 12 proposes a simple, although very speculative scheme for a sequence of processes, which might be at work. First, from the earthquake preparation area an upward electric charges flux is produced that will flow along the magnetic field line. This flux, in turn, will produce the corresponding plasma enhancements just above the epicentre and its conjugate point: in this representation, CSES, that flew at around 2 LT detected only the southern increase of electron density, while Swarm Charlie, that flew at around 3 LT (one hour after) was able to detect both enhancements. The reason of this difference could be twofold. The different inclination of CSES orbit, i.e. its track, was slightly more inclined with respect to the main meridian, better followed by Swarm satellites. This would have allowed CSES to detect only the southern crest of the anomaly. Alternatively, in case of a non-perfectly symmetric anomaly in altitude, the CSES higher altitude would have limited the detection of the northern anomaly, maybe placed at lower altitude with respect to the southern anomaly.

We understand that this explanation is highly speculative, but, if the origin of the detected anomalies is really lithospheric, the processes here described will be possibly occurring.

A visual inspection of the electron density profiles acquired by CSES satellite in April, August and September seems to suggest that some Ne anomalies preceded the main seismic events (M5.5 +) from 1 to 10 days before the occurrence of the events. Unfortunately, the available interval of CSES Ne data is not sufficient to make a confutational analysis to confirm or not this speculation. A similar analysis performed on magnetic data acquired by HPM onboard CSES shows a possible good seismo-induced magnetic anomaly on August 14th, 2018.

Fig. 13a–c report the behavior of the cumulative number of anomalies that we detect in lithosphere, atmosphere, and ionosphere, respectively. For this comparative analysis, we take into account only the observables that have continuous availability, to be sure that the eventual variations in time series are not due to a gap of data. We took into account the seismological analysis on earthquake catalogue, atmospheric investigation on ECMWF and MERRA-2 climatological datasets and the study of the ionosphere with the Swarm constellation. In a conservative approach, in this overview we exclude CSES data, as the complete release is not yet available for the full analysed interval. From the same figure, we can notice that there are two periods with an increase of atmospheric anomalies about 6 months and about 3.7 months before the earthquake occurrence. About 2.7 months before the earthquake a rapid increase of ionospheric anomalies starts. These times of anticipation of the mainshock could seem too much long, but the atmospheric and ionospheric anomalies of 3.7 months and 2.7 months before the event are completely compatible with the general empirical law proposed by Rikitake (1987) that estimates a mean anticipation time of about 90 days for magnitude 7.5 earthquakes. The time-closest anomalies to the mainshock are seismic activation and acceleration. It is interesting to note that, in principle, the analysis of the increase of seismic activity could be the last technique to definitively warn a region in future earthquake prediction platforms, nevertheless not all earthquakes are preceded by foreshocks and/or seismic acceleration, so the method cannot be always successfully applied. Probably the "key" to resolve the issue is to integrate the present seismic study with a quiescence analysis that seems to work also in case of lack of significant foreshocks and it gives an anticipation time between some months and more than one year (e.g. Di Giovambattista and Tyupkin, 2000; Gentili, 2010). The seismic quiescence usually precedes the alterations in atmosphere and ionosphere (e.g. Marchetti et al., 2019b), underlining the starting point of the precursory effects. We could say that seismic quiescence, and alterations in atmosphere and ionosphere are preparation phase effects, likely occurring in a large area, approximated by the Dobrovolsky's area, while the final seismic acceleration (as we found in this work) is just the final part of the main lithospheric final rupture, i.e. the mainshock. In this work, we could not search seismic quiescence in the data because the M_c of the used USGS catalogue is too high for this particular technique.

5. Conclusions

This work supports the study of the different Lithosphere-Atmosphere-Ionosphere Coupling models like the one provided by Pulinets and Ouzounov (2011), identifying anomalies before in the atmosphere and after in ionosphere during the whole analysed period. Such type of phenomena could be induced in different ways, or "channels" (as called by Yang et al., 2019). We discuss a simple electric model, in some way analogous with the electrostatic channel by Freund et al. (2011), but others can be reasonable as well. For instance, the chemical channel, by the release of some gas and radon in atmosphere that, in turn, could activate a chain of processes, like the formation of aerosol particles (as found in this paper), clouds, warming of Earth's surface (possibly detected in skt analysis). Finally, by global alterations of electric circuit (e.g. Kuo et al., 2014, 2018) between atmosphere and ionosphere, it is possible to identify some electromagnetic disturbance up to the ionosphere (possibly detected in this paper by Swarm and CSES satellites). Recently, Yang et al. (2019) are more in favour of a third channel, the atmospheric gravity wave/ acoustic wave channel.

The anomaly of the August 2nd, 2018 in atmosphere and ionosphere could be described in an alternative model with a rapid coupling mechanism, induced, for example, by electromagnetic very low frequency emissions from seismogenic fault. This type of analysis could open a new perspective for the LAIC models by confirming or refuting some proposed mechanisms, and shedding light on the real physical mechanism which could be involved.

Declaration of Competing Interest

The authors declare that they have no known competing financial interests or personal relationships that could have appeared to influence the work reported in this paper.

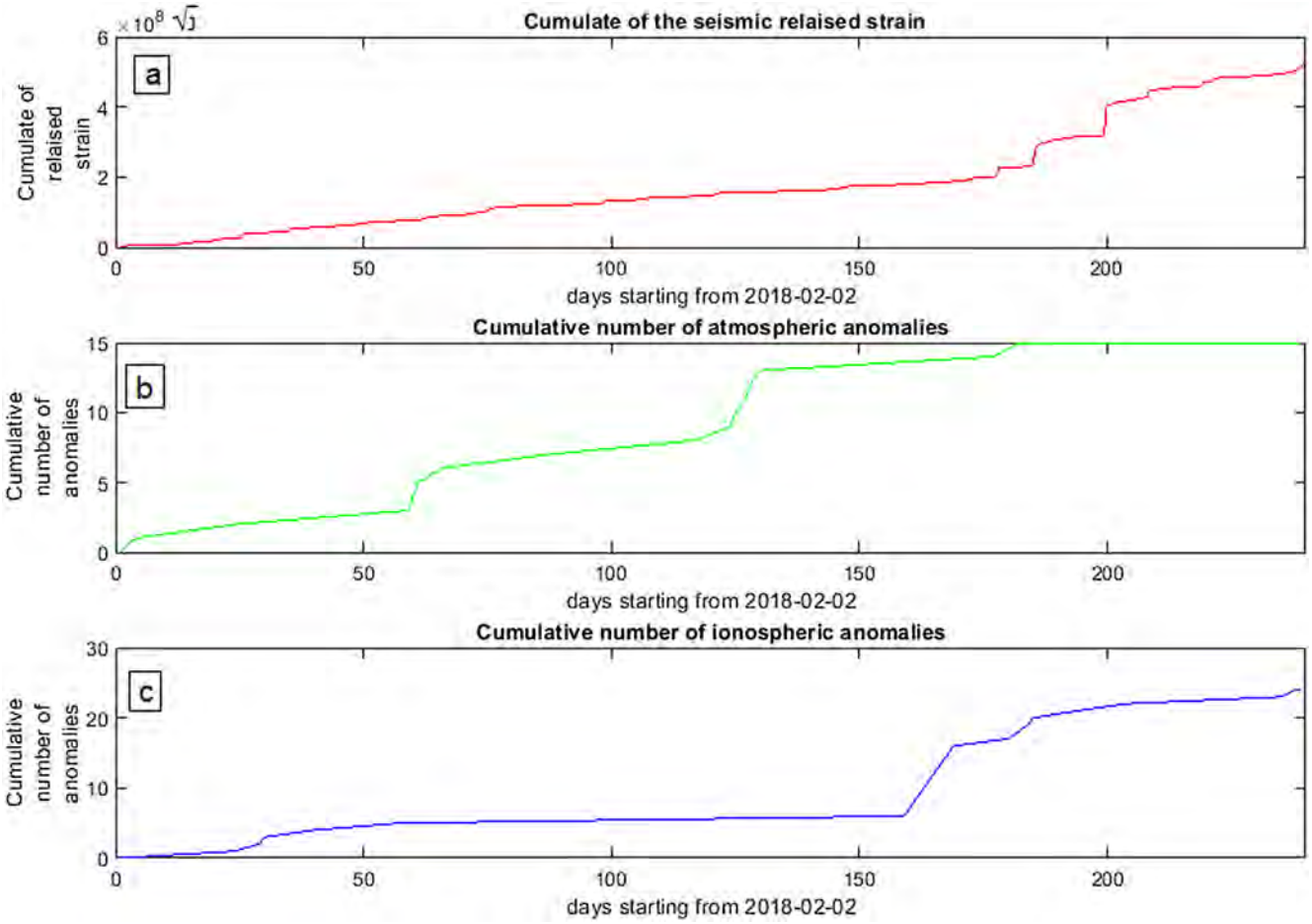

Fig. 13. Summary of the different analyses investigating the lithosphere (a), the atmosphere (b) and the ionosphere (c). In particular, (a) shows the cumulative relaised strain in the Dobrovolsky's area for shallow M4.5 + earthquakes (depth ≤ 50 km); (b) reports the cumulative number of anomalies detected in atmosphere for skt, tcwv and aerosol; finally panel (c) reports the cumulative number of ionospheric anomalies detected by Swarm satellites. When in the same days two or more methods detect a magnetic anomaly it counts only once as the observable is unique.

Acknowledgements

This work made use of the data from CSES mission, a project funded by China National Space Administration (CNSA) and China Earthquake Administration (CEA) (both in China) in collaboration with Italian Space Agency (ASI) and Istituto Nazionale di Fisica Nucleare (INFN) (both in Italy).

This work was undertaken in the framework of the ESA-funded project SAFE (Swarm for Earthquake study), and under the LIMADOU-Science, a project funded by the Italian Space Agency (ASI).

The authors thank the developers of ZMap 7 software tools (Wiemer, 2001) used in this paper for some earthquake data representation.

The authors thank prof. Francisco Javier Pavón Carrasco for his precious contribution to the development of some parts of the used codes, Prof. Roberto Battiston and Dr. Piero Diego for their useful suggestions and prof. Mehdi Akhoondzadeh for the interesting indications.

Appendix A. Supplementary material

Supplementary data to this article can be found online at https://doi.org/10.1016/j.jseaes.2019.104097.

References

Abdu, M.A., Kherani, E.A., Batista, I.S., Sobral, J.H.A., 2009. Equatorial evening prereversal vertical drift and spread F suppression by disturbance penetration electric fields. Geophys. Res. Lett. 36, L19103. https://doi.org/10.1029/2009GL039919.

Alfonsi, L., Ambroglini, F., Ambrosi, G., Ammendola, R., Assante, D., Badoni, D., Belyaev, V.A., Burger, W.J., Cafagna, A., Cipollone, P., Consolini, G., Conti, L., Contin, A., De Angelis, E., De Donato, C., De Franceschi, G., De Santis, A., De Santis, C., Diego, P., Durante, M., Fornaro, C., Guandalini, C., Laurenti, G., Laurenza, M., Lazzizzera, I., Lolli, M., Manea, C., Marcelli, L., Marcucci, F., Masciantonio, G., Osteria, G., Palma, F., Palmonari, F., Panico, B., Patrizii, P., Picozza, P., Pozzato, M., Rashevskaya, I., Ricci, M., Rovituso, M., Scotti, V., Sotgiu, A., Sparvoli, R., Spataro, B., Spogli, L., Tommasino, F., Ubertini, P., Vannaroni, G., Xuhui, S., Zoffoli, Z., Collaboration, The CSES-LIMADOU, 2017. The HEPD particle detector and the EFD electric field detector for the CSES satellite. Radiat. Phys. Chem. 137, 187–192. https://www.sciencedirect.com/science/article/pii/S0969806X16308301.

Aliano, C., Corrado, R., Filizzola, C., Genzano, N., Pergola, N., Tramutoli, V., 2008. Robust TIR satellite techniques for monitoring earthquake active regions: limits, main achievements and perspectives. Ann. Geophys. 51 (1), 303–318.

Akhoondzadeh, M., De Santis, A., Marchetti, D., Piscini, A., Cianchini, G., 2018. Multi precursors analysis associated with the powerful Ecuador (MW = 7.8) earthquake of 16 April 2016 using Swarm satellites data in conjunction with other multi-platform satellite and ground data. Adv. Space Res. 61 (1), 248–263.

Akhoondzadeh, M., De Santis, A., Marchetti, D., Piscini, A., Jin, S., 2019. Anomalous seismo-LAI variations potentially associated with the 2017 Mw = 7.3 Sarpol-e Zahab (Iran) earthquake from Swarm satellites, GPS TEC and climatological data. Adv. Space Res. 64, 143–158. https://doi.org/10.1016/j.asr.2019.03.020.

Akhoondzadeh, M., Parrot, M., Saradjian, M.R., 2010a. Electron and ion density variations before strong earthquakes (M > 6.0) using DEMETER and GPS data. Nat. Hazards Earth Syst. Sci. 10, 7–18. https://doi.org/10.5194/nhess-10-7-2010.

Akhoondzadeh, M., Parrot, M., Saradjian, M.R., 2010b. Investigation of VLF and HF waves showing seismo-ionospheric anomalies induced by the 29 September 2009 Samoa earthquake (Mw = 8.1). Nat. Hazards Earth Syst. Sci. 10, 1061–1067. https://doi.org/10.5194/nhess-10-1061-2010.

Bilitza, D., Altadill, D., Truhlik, V., Shubin, V., Galkin, I., Reinisch, B., Huang, X., 2017. International reference ionosphere 2016: From ionospheric climate to real-time weather predictions. Space Weather 15 (2), 418–429.

Cicerone, R.D., Ebel, J.E., Britton, J., 2009. A systematic compilation of earthquake

precursors. Tectonophysics 476, 371–396.
Chen, Y., Liu, L., Le, H., 2008. Solar activity variations of nighttime ionospheric peak electron density. J. Geophys. Res. 113, A11306. https://doi.org/10.1029/2008JA013114.
Cheng, B., Zhou, B., Magnes, W., Lammegger, R., Pollineger, A., 2018. High Precision magnetometer for geomagnetic exploration onboard of the China seismo-electromagnetic satellite. Sci. China Technol. Sci. 61 (5), 659–668. https://doi.org/10.1007/s11431-018-9247-6.
Dee, D.P., Uppala, S.M., Simmons, A.J., Berrisford, P., Poli, P., Kobayashi, S., Andrae, U., Balmaseda, M.A., Balsamo, G., Bauer, P., Bechtold, P., Beljaars, A.C.M., van de Berg, L., Bidlot, J., Bormann, N., Delsol, C., Dragani, R., Fuentes, M., Geer, A.J., Haimberger, L., Healy, S.B., Hersbach, H., Hólm, E.V., Isaksen, L., Kållberg, P., Köhler, M., Matricardi, M., McNally, A.P., Monge-Sanz, B.M., Morcrette, J.-J., Park, B.-K., Peubey, C., de Rosnay, P., Tavolato, C., Thépaut, J.-N., Vitart, F., 2011. The ERA-Interim reanalysis: configuration and performance of the data assimilation system. Q.J.R. Meteorol. Soc. 137, 553–597. https://doi.org/10.1002/qj.828.
De Santis, A., De Franceschi, G., Spogli, L., Perrone, L., Alfonsi, L., Qamili, E., Cianchini, G., et al., 2015a. Geospace perturbations induced by the Earth: the state of the art and future trends. Phys. Chem. Earth 85–86, 17–33.
De Santis, A., Cianchini, G., Di Giovambattista, R., 2015b. Accelerating moment release revisited: Examples of application to Italian seismic sequences. Tectonophysics 639, 82–98. https://doi.org/10.1016/j.tecto.2014.11.015.
De Santis, A., Balasis, G., Pavón-Carrasco, F.J., Cianchini, G., Mandea, M., 2017. Potential earthquake precursory pattern from space: the 2015 Nepal event as seen by magnetic Swarm satellites. Earth Planet. Sci. Lett. 461, 119–126.
De Santis, A., et al., 2019. Geosystemics view of earthquakes. Entropy 21, 412. https://doi.org/10.3390/e21040412.
Di Giovanbattista, R., Tyupkin, Yu.S., 2000. Spatial and temporal distribution of seismicity before the Umbria-Marche September 26, 1997 earthquakes. J. Seism. 4, 589–598.
Dobrovolsky, I.P., Zubkov, S.I., Miachkin, V.I., 1979. Estimation of the size of earthquake preparation zones. PAGEOPH 117, 1025. https://doi.org/10.1007/BF00876083.
Donner, R.V., Potirakis, S.M., Balasis, G., Eftaxias, K., Kurths, J., 2015. Temporal correlation patterns in pre-seismic electromagnetic emissions reveal distinct complexity profiles prior to major earthquakes. Phys. Chem. Earth, Parts A/B/C,. https://doi.org/10.1016/j.pce.2015.03.008.
Fejer, B.G., Blanc, M., Richmond, A.D., 2017. Post-storm middle and low-latitude ionospheric electric fields effects. Space Sci. Rev. 206 (1–4), 407–429.
Fraser-Smith, A.C., Bernardi, A., McGill, P.R., Ladd, M.E., Helliwell, R.A., Villard Jr., O.G., 1990. Low-frequency magnetic field measurements near the epicenterr of the Ms 7.1 Loma Prieta Earthquake. GRL 17 (9), 1465–1468. https://doi.org/10.1029/GL017i009p01465.
Freund, F., 2011. Pre-earthquake signals: underlying physical processes. J. Asian Earth Sci. 383–400.
Friis-Christensen, E., Luhr, H., Hulot, G., 2006. Swarm: A constellation to study the Earth's magnetic field, Earth Plan. Space 58, 351–358.
Gelaro, R., McCarty, W., Suárez, M.J., Todling, R., Molod, A., Takacs, L., Randles, C.A., Darmenov, A., Bosilovich, M.G., Reichle, R., Wargan, K., Coy, L., Cullather, R., Draper, C., Akella, S., Buchard, V., Conaty, A., da Silva, A.M., Gu, W., Kim, G.-K., Koster, R., Lucchesi, R., Merkova, D., Nielsen, J.E., Partyka, G., Pawson, S., Putman, W., Rienecker, M., Schubert, S.D.c., Sienkiewicz, M., Zhao, B., 2017. The modern-era retrospective analysis for research and applications, version 2 (MERRA-2). American Meteorological Society - Modern-Era Retrospective analysis for Research and Applications version 2 (MERRA-2) special collection.
Gentili, S., 2010. Distribution of seismicity before large earthquakes in Italy in the time interval 1994–2004. Pure Appl. Geoph. 167, 933–958.
Han, P., Hattori, K., Hirokawa, M., Zhuang, J., Chen, C.-H., Febriani, F., Yamaguchi, H., Yoshino, C., Liu, J.-Y., Yoshida, S., 2014. Statistical analysis of ULF seismomagnetic phenomena at Kakioka, Japan, during 2001–2010. J. Geophys. Res. Space Phys. 119, 4998–5011. https://doi.org/10.1002/2014JA019789.
Hanson, W.B., Moffett, R.J., 1966. Ionization transport effects in the equatorial F region. J. Geophys. Res. 71, 5559–5572. https://doi.org/10.1029/JZ071i023p05559.
He, Y., Yang, D., Quian, J., Parrot, M., 2011. Response of the ionosphere electron density to different types of seismic events. Nat. Hazard Earth Syst., Sci. 11, 2173–2180.
Heki, K., 2011. Ionospheric electron enhancement preceding the 2011 Tohoku-Oki Earthquake. Geophys. Res. Lett. 38 (17), 1–5. https://doi.org/10.1029/2011GL047908.
Kagan, Yan Y., 2003. Accuracy of modern global earthquake catalogs. Phys. Earth Planet. Inter. 135 (2–3), 173–209. https://doi.org/10.1016/S0031-9201(02)00214-5.
Kamogawa, M., Kakinami, Y., 2013. Is an ionospheric electron enhancement preceding the 2011 Tohoku-oki earthquake a precursor? J. Geophys. Res. Space Physics 118, 1–4. https://doi.org/10.1002/jgra.50118.
Kanamori, H., Anderson, D.L., 1975. Theoretical basis of some empirical relations in seismology. Bull. Seis. Soc. Am. 65 (5), 1073–1095.
Kuo, C.L., Lee, L.C., Huba, J.D., 2014. An improved coupling model for the lithosphere-atmosphere-ionosphere system. J. Geophys. Res. Space Phys. 119, 3189–3205. https://doi.org/10.1002/2013JA019392.
Kuo, C.L., Ho, Y.Y., Lee, L.C., 2018. Electrical Coupling Between the Ionosphere and Surface Charges in the Earthquake Fault Zone. In: Chapter of the book Pre-Earthquake Processes. Wiley. https://doi.org/10.1002/9781119156949.ch7.
Jin, S., 2018. Two-mode ionospheric disturbances following the 2005 northern California offshore earthquake from GPS measurements. J. Geophys. Res. Space Phys. 123. https://doi.org/10.1029/2017JA025001.
Li, M., Parrot, M., 2013. Statistical analysis of an ionospheric parameter as a base for earthquake prediction. J. Geophys. Res. Space Phys. 118, 3731–3739. https://doi.org/10.1002/jgra.50313.
Liu, Q., Shen, X., Zhang, J., Li, M., 2019. Exploring the abnormal fluctuations of atmospheric aerosols before the 2008 Wenchuan and 2013 Lushan earthquakes. Adv. Space Res. https://doi.org/10.1016/j.asr.2019.01.032.
MacDouglas, J.W., 1969. The equatorial ionospheric anomaly and the equatorial electrojet. Radio Sci. 4 (9), 805–810.
Marchetti, D., Akhoondzadeh, M., 2018. Analysis of Swarm satellites data showing seismo-ionospheric anomalies around the time of the strong Mexico (Mw = 8.2) earthquake of 08 September 2017. Adv. Space Res. https://doi.org/10.1016/j.asr.2018.04.043.
Marchetti, D., De Santis, A., D'Arcangelo, S., Poggio, F., Jin, S., Piscini, A., A. Campuzano, S., 2019a. Magnetic field and electron density anomalies from Swarm satellites preceding the major earthquakes of the 2016–2017 Amatrice-Norcia (Central Italy) seismic sequence. Pure Appl. Geophys. https://doi.org/10.1007/s00024-019-02138-y.
Marchetti, D., De Santis, A., D'Arcangelo, S., Poggio, F., Piscini, A., A. Campuzano, S., Werneck, V., 2019b. Pre-earthquake chain processes detected from ground to satellite altitude in preparation of the 2016–2017 seismic sequence in Central Italy. Remote Sens. Environ. 229, 93–99. https://doi.org/10.1016/j.rse.2019.04.033.
Mignan, A., King, G.C.P., Bowman, D., 2007. A mathematical formulation of accelerating moment release based on the stress accumulation model. J. Geophys. Res. 112, B07308. https://doi.org/10.1029/2006JB004671.
Molchanov, O., Hayakawa, M., 2008. Seismo Electromagnetics and Related Phenomena: History and latest results. TerraPub, Tokyo, pp. 189.
Molchanov, O.A., Kopytenko, YuA., Voronov, P.M., Kopytenko, E.A., Matiashvili, T.G., Fraser-Smith, A.C., Bernardi, A., 1992. Results of ULF magnetic field measurements near the epicenters of the Spitak (Ms = 6.9) and Loma Prieta (Ms = 7.1) earthquakes: comparative analysis. Geophys. Res. Lett. 19 (14), 1495–1498. https://doi.org/10.1029/92GL01152.
Nêmec, F., Santolik, O., Parrot, M., Berthelier, J.J., 2008. Spacecraft observations of electromagnetic perturbations connected with seismic activity. Geophys. Res. Lett. 35, L05109. https://doi.org/10.1029/2007GL032517.
Oikonomou, C., Haralambous, H., Muslim, B., 2016. Investigation of ionospheric TEC precursors related to the M7.8 Nepal and M8.3 Chile earthquakes in 2015 based on spectral and statistical analysis. Nat. Hazards 83 (Suppl 1), 97. https://doi.org/10.1007/s11069-016-2409-7.
Parrot, M., 2013. Satellite observations of ionospheric perturbations related to seismic activity. In: Hayakawa, M. (Ed.), Earthquake Prediction Studies: Seismo Electromagnetics. TERRAPUB, Tokyo, pp. 1–16.
Parrot, M., Li, M., 2015. DEMETER results related to seismic activity. Radio Sci. Bull. No 355 18–25.
Pinheiro, K.J., Jackson, A., Finlay, C.C., 2011. Measurements and uncertainties of the occurrence time of the 1969, 1978, 1991, and 1999 geomagnetic jerks. Geochem. Geophys. Geosyst. 12, Q10015.
Piša, D., Nêmec, F., Santolik, O., Parrot, M., Rycroft, M., 2013. Additional attenuation of natural VLF electromagnetic waves observed by the DEMETER space-craft resulting from preseismic activity. J. Geophys. Res. Space Phys. 118. https://doi.org/10.1002/jgra.50469.
Piscini, A., De Santis, A., Marchetti, D., Cianchini, G., 2017. A multi-parametric climatological approach to study the 2016 Amatrice-Norcia (Central Italy) earthquake preparatory phase. Pure Appl. Geophys. 174 (10), 3673–3688.
Piscini, A., Marchetti, D., De Santis, A., 2019. Multi-parametric climatological analysis associated with global significant volcanic eruptions during 2002–2017. Pure Appl. Geophys. https://doi.org/10.1007/s00024-019-02147-x.
Povero, G., Alfonsi, L., Spogli, L., Di Mauro, D., Cesaroni, C., Dovis, F., Floury, N., 2017. Ionosphere monitoring in South East Asia in the ERICA study. Navigation: J. Instit. Navig. 64 (2), 273–287.
Pulinets, S., Ouzounov, D., 2011. Lithosphere-Atmosphere- ionosphere coupling (LAIC) model-an unified concept for earthquake precursors validation. J. Asian Earth Sci. 41 (4–5), 371–382.
Rikitake, T., 1987. Earthquake precursors in Japan: precursor time and detectability. Tectonophysics 136, 265–282.
Shen, X., et al., 2018. Introduction to special section on the China seismo-electromagnetic satellite and initial results. Earth Planet. Phys. 2 (6), 439–443.
Spogli, L., Cesaroni, C., Di Mauro, D., Pezzopane, M., Alfonsi, L., Musicò, E., ... & Linty, N. (2016). Formation of ionospheric irregularities over Southeast Asia during the 2015 St. Patrick's Day storm. Journal of Geophysical Research: Space Physics, 121(12).
Thébault, E., et al., 2015. International geomagnetic reference field: the 12th generation. Earth Planets Space. https://doi.org/10.1186/s40623-015-0228-9.
Tramutoli, V., Corrado, R., Filizzola, C., Genzano, N., Lisi, M., Pergola, N., 2015. From visual comparison to Robust Satellite Techniques: 30 years of thermal infrared satellite data analyses for the study of earthquake preparation phases. Bollettino di Geofisica Teorica ed Applicata 56 (2), 167–202. https://doi.org/10.4430/bgta0149.
USGS U.S. Geological Survey, 2018, National Earthquake Information Center, accessed November 15, 2018 at the URL https://earthquake.usgs.gov/earthquakes/search and for specific information about Indonesia M7.5 2018 earthquake: https://earthquake.usgs.gov/earthquakes/eventpage/us1000h3p4/executive.
Venkatesh, K., Tulasi Ram, S., Fagundes, P., Seemala, G.K., Batista, I., 2017. Electrodynamic disturbances in the Brazilian equatorial and low-latitude ionosphere on St. Patrick's Day storm of 17 March 2015. J. Geophys. Res. 122 (4), 4553.
Walker, G.O., Ma, J.H.K., Golton, E., 1994. The equatorial ionospheric anomaly in electron content from solar minimum to solar maximum for South East Asia. Ann. Geophys. 12 (2–3), 195–209.
Wei, Y., Zhao, B., Li, G., Wan, W., 2015. Electric field penetration into Earth's ionosphere: a brief review for 2000–2013. Sci. Bull. 60 (8), 748–761.
Wiemer, S., 2001. A software package to analyze seismicity: ZMAP. Seismol. Res. Lett. 72 (3), 373–382. https://doi.org/10.1785/gssrl.72.3.373.

Yan, R., Guan, Y.B., Shen, X.H., Huang, J.P., Zhang, X.M., Liu, C., Liu, D.P., 2018. The Langmuir Probe onboard CSES: data inversion analysis method and first results. Earth Planet. Phys. 2 (6), 479–488. https://doi.org/10.26464/epp2018046.

Yan, R., Parrot, M., Pinçon, J.-L., 2017. Statistical study on variations of the ionospheric ion density observed by DEMETER and related to seismic activities. J. Geoph. Res. Space Phys. 122. https://doi.org/10.1002/2017JA024623.

Yang, S.-S., Asano, T., Hayakawa, M., 2019. Abnormal gravity wave activity in the stratosphere prior to the 2016 Kumamoto earthquakes. J. Geoph. Res. Space Phys. 124, 1410–1425. https://doi.org/10.1029/2018JA026002.

Zhang, Q., Guo, F., Zhao, L., Wu, Y., 2017. Geodynamics of divergent double subduction: 3-D numerical modeling of a Cenozoic example in the Molucca Sea region, Indonesia. J. Geophys. Res. Solid Earth 122, 3977–3998. https://doi.org/10.1002/2017JB013991.